# Determination of the natural deuterium distribution of fatty acids by application of 2H 2D-NMR in liquid crystals: fundamentals, advances, around and beyond

Philippe Lesot

▶ **To cite this version:**

Philippe Lesot. Determination of the natural deuterium distribution of fatty acids by application of 2H 2D-NMR in liquid crystals: fundamentals, advances, around and beyond. Liquid Crystals, 2020, 47 (13), pp.1889-1910. 10.1080/02678292.2019.1613685 . hal-02308723

**HAL Id: hal-02308723**
**https://hal.science/hal-02308723**

Submitted on 2 Dec 2020

**HAL** is a multi-disciplinary open access archive for the deposit and dissemination of scientific research documents, whether they are published or not. The documents may come from teaching and research institutions in France or abroad, or from public or private research centers.

L'archive ouverte pluridisciplinaire **HAL**, est destinée au dépôt et à la diffusion de documents scientifiques de niveau recherche, publiés ou non, émanant des établissements d'enseignement et de recherche français ou étrangers, des laboratoires publics ou privés.

# Determination of the natural deuterium distribution of fatty acids by application of $^{2}$H 2D-NMR in liquid crystals: Fundamentals, advances, around and beyond

**Philippe Lesot*'**

*Laboratoire de RMN en Milieu Orienté, UMR CNRS 8182, ICMMO, Bât. 410, Université de Paris-Saclay, F-91405 Orsay cedex, France.*

***Special issue in memory of Prof. Zeev Luz (1932 - 2018)***

**ABSTRACT:**

Based on pioneering work reported in the 1980's by Martin and co-workers, experimental investigation of the site-specific, natural ($^{2}$H/$^{1}$H) isotope fractionation in bioproducts by natural abundance deuterium 1D-NMR (NAD 1D-NMR) spectroscopy is the method of choice to understand the enzymatic mechanisms leading to their synthesis or transformation, but also to determine their geographical or botanical origins. This approach, known as $^{2}$H-SNIF-NMR$^{TM}$ method, is also an effective tool in the fight against the counterfeiting of molecules of economical interests. However, the use of achiral isotropic solvents has two significant disadvantages that reduce accessible isotopic information: a rate of overlap of signals generally too high for complex analytes and the absence of spectral discrimination of enantiotopic directions in prochiral compounds. Both drawbacks can be overcome by replacing liquid solvents with chiral liquid crystals (CLC). In this review, we overview the theoretical basis and the analytical advantages of anisotropic NAD (ANAD) 2D-NMR using polypeptide-based, lyotropic CLCs as enantiodiscriminating ordered NMR solvents. We discuss how and why ANAD 2D-NMR can provide a robust alternative to the conventional method of determining isotopic ratios, $(^{2}H/^{1}H)_{i}$, particularly when applied to long-chain fatty acids or homogeneous triglycerides. Various applicative aspects are presented.

**KEYWORD:**

Deuterium; natural abundance; SNIF-NMR; 2D-NMR; isotope fractionation; chiral liquid crystal; fatty acid; triglyceride.

**TYPE OF ARTICLE:** Review article

**CORRESPONDING AUTHOR:** Philippe Lesot Philippe.lesot@u-psud.fr

Orcid.org/0000-0002-5811-7530

POST-PRINT

## 1. Introduction

$^{1}H$, $^{2}H$, $^{13}C$, $^{15}N$, …. NMR spectroscopies and their various multinuclear-correlation, multidimensional (nD) experiments are essential tools for the modern structural analysis of complex natural or synthetic molecules. In another analytical field, NMR spectroscopy is also a powerful technique for determining, for example, the proportion of components of dynamic molecular mixtures (conversion rate, reaction monitoring, ...) or stable mixtures (enantiomeric/diastereoisomeric excess), including the case of isotopomeric mixtures ($^{2}H/^{1}H$, $^{13}C/^{12}C$, $^{15}N/^{14}N$, $^{17}O/^{16}O$, …) from which unique data on the natural isotopic profile of analytes can be extracted [**1**].

Among pairs of interesting stable nuclear isotopes, the quantitative detection of deuterium nuclei at natural abundance level by NMR (NAD NMR) in isotropic solvents is a method of choice for the study of site-specific isotopic fractionation of deuterium/hydrogen, $(^{2}H/^{1}H)_i$, in biomolecules for instance. Experimentally pioneered and then intensively developed by Gérard and Maryvone Martin and their team in early 80's, this methodology, named as Site-specific Natural Isotope Fractionation (or SNIF-NMR™) was initially proposed for the analysis of wine ethanol in the frame of fight against excessive chaptalisation practice [**2,3**]. It was then extended to various domains (authenticity/traceability investigations) [**4,5**], and wide range of analytes of economical interest, such as vanillin or frambinone (food aroma), for instance [**6,7,8**]. Based on the analytical abilities of this methodology led to the creation of Eurofins Scientific international compagny, the world leader in isotopic analysis and analytical standards, in 1987.

Despite significant successes, the historical SNIF-NMR™ approach, like all analytical tools, possesses intrinsic limitations that can be overcome by replacing isotropic liquid solvents with lyotropic chiral liquids crystals (CLCs). As we will see in this review, the use of oriented chiral phases to $^{2}H$ isotopic analysis by NMR can be considered as a shift of paradygm in the domain, because in the same NMR experiment, we can access to new NMR interactions averaged out to zero in liquids (anisotropic interactions), which in turn can be related to some fundamental properties of molecules, including their stereochemistry.

To illustrate an exciting facet of the analytical potential of anisotropic NMR, which has been explored very early in the NMR history by some curious and outstanding spectroscopists as Zeev Luz [**9**], we will present in this review the original contribution of polypeptide-based CLCs to the study of the site-specific natural hydrogen fractionation. As illustrating examples, the extended family of essential fatty acids (FAs) in the form of unsaturated fatty acids FAs (ω-3, ω-6, ω-9), C-14 to C-18 saturated AG, triglycerides, ...., will be proposed as a case study.

POST-PRINT

## 2. Specificities of Hydrogen fractionation

The isotope ratio value ($^2H/^1H$) using (fresh) ocean water molecules (known as V-SMOW value: Vienna-Standard Mean Ocean Water) has been set at $1.5576 \times 10^{-2}$% (155,76 ppm) for hydrogen atoms. This value was promulgated by the International Atomic Energy Agency (based in Vienna) in 1968, and is still used as international standard value [**10**]. However, in natural hydrogenated compounds, significant changes in the isotope ratios ($^2H/^1H$) (up to 50%) can be observed at its different hydrogenated sites. This non-statistical intramolecular distribution of hydrogen isotope means that the content of different monodeuterated isotopomers depends on the deuterium-substituted position. These site-specific intramolecular variations define the isotopic fractionation of a molecule and characterize its isotopic profile. These profiles are unique molecular fingerprints that can be related to the geographical or botanical origin of a compound, and hence provide data sources in the fight against counterfeiting (adulteration, substitution, imitation of premium products), for instance [**11**]. From a theoretical point of view, the analysis of the isotopic profiles of a substrate/product pair can also makes it possible to study the primary or secondary kinetic isotopic effects (KIEs) [**12**], to identify hydrogen deuterium) sources, and thus to understand the enzymatic mechanisms leading to the synthesis/transformation of natural compounds [**13,14,15,16**].

## 3. The classical $^2H$ SNIF-NMR™ protocol

The principle of SNIF-NMR™ protocol is to record proton-decoupled NAD 1D spectra (NAD-{$^1H$} NMR) spectra in a non-deuterated isotropic solvent (or a solvent mixture: $CCl_4/CHCl_3$/pyridine) in the presence of an internal reference chemical substance such as tetramethyl urea (TMU) (primary reference) whose ratio $(^2H/^1H)_{TMU}$ is precisely calibrated [**17**]. Alternatively to chemical references, the use of an electronic reference inducing a $^2H$ NMR signal (frequency controlled) on spectrum has been developed. This method, called Electronic Reference To access In vivo Concentrations (ERECTIC) has the advantage of being able to position the reference signal in spectrum free of all signals of the analyte [**17**]. Whatever the type of internal reference used, NAD-{$^1H$} NMR spectra are recorded with quantitative conditions that allows reliable measurements to be obtained, in particularly by using a recycling delay with $T_{recycling} > 5 \times T_1(^2H)$ where $T_1(^2H)$ is the longest longitudinal relaxation time $^2H$ of the sample (associated to the analyte or the chemical reference).

Knowing the mass (m) of the mixture components (analyte and reference), their molecular weight (M), their stoichiometric hydrogen site number i (P), and their peak surface (S) measured on the NAD spectra, the isotopic ratio $(^2H/^1H)_i$ (value in ppm) is evaluated by **Eq. 1** as [**2,18**],

POST-PRINT

$$= \frac{P_{ref} \times m_{ref} \times M_{anal} \times S_{i,anal}}{P_{i,anal} \times m_{anal} \times M_{ref} \times S_{ref}} \times \left(\frac{^2H}{^1H}\right)^{iso}_{ref} \quad (\mathbf{1})$$

where $(^2H/^1H)_i$ is the isotopic ratio of the calibrated reference.

Since its introduction, the SNIF-NMR™ protocol has been widely applied worldwide for many isotope-based analytical applications [**19,20,21**], and has demonstrated its ability to provide critical isotopic information on analytes of interest. Very recently, the same principle has been extended to the analysis of the natural isotopic $(^{13}C/^{12}C)_i$ fractionation, but this new development is beyond the scope of this review [**22,23**].

## 4. Analytical limitations and alternatives

While SNIF-NMR™ was successfully applied for analysing small functionalised organic molecules, this protocol has two major disadvantages. First of all, the low dispersion of $^2H$ signals on isotropic $^2H$ NMR spectra due to the low gyromagnetic ratio of deuterons ($\gamma(^2H) = \gamma(^1H)/6.515$) makes difficult the analysis of low-polarity molecules containing numerous inequivalent $^2H$ sites, even at very high magnetic fields. Second, the use of achiral isotropic solvents does not allow the isotope ratios associated with pro-*R*/pro-*S* hydrogen enantiotopic sites (see **Figure 1**) to be measured. Under both circumstances, the amount of isotopic information experimentally available by NMR can be significantly incomplete, and lead to only partial knowledge of the $(^2H/^1H)$ isotopic profile.

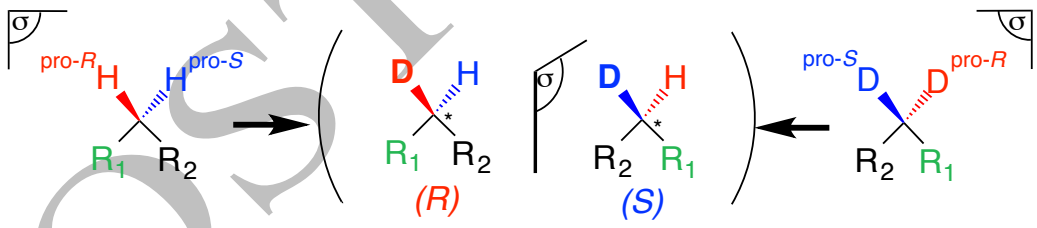


**Figure 1.** Example of pair of (D/H) isotopic enantiomers, *R*/*S*, ($C_1$-symmetry chiral molecule) detected by NAD NMR (monodeuterated enantio-isotopomers) associated to enantiotopic directions, pro-*R*/pro-*S*, ($CH_2$ or $CD_2$) of hydrogenated or deuterated prochiral analogous ($C_s$ symmetry).

To limit excessive overlaps of $^2H$ singlets on NAD NMR spectra, we can work at higher $^2H$ Larmor frequency by increasing the magnetic field strength, $B_0$, but this solution does not avoid fortuitous equivalent hydrogen positions (pseudo-isochronism) as in case of two aromatic sites of vanillin [**6,24**]. A more pragmatical approach to problem, based on the chemical fragmentation of the analyte into different parts (which are then analysed separately), can be adopted. As we will see below, this strategy was applied

POST-PRINT

first for the analysis of PUFAs [**25**]. In practice, this solution is, however, really usable if the cleavage of chemical functions can be easily activated (*e.g.* a double/triple bond). In addition, this chemical breakdown induces two important drawbacks: (i) the lost of $(^2H/^1H)_i$ isotope information ratios at cutting sites; (ii) a possible modification in isotope ratios at sites adjacent to the cut (induced fractionation). Finally, a third way exists and consists in exploiting the $^2H$ residual quadrupolar couplings, $^2H$-RQC, (specific to nuclei with $I > 1/2$) which can be detected by replacing isotopic solvents with oriented media as lyotropic liquid crystals (LLC) (see **Section 5.1**). Interestingly, this third original alternative opens also the opportunity to discriminate the enantiotopic directions in prochiral molecules, if the LC used is chiral (see **Section 5.2**) [**26**].

## 5. Specificities of the anisotropic NAD NMR (ANAD NMR)

### *5.1 $^2H$ Residual quadrupolar coupling*

In LCs (achiral or chiral), any solutes are partially orientationally ordered in average. As a result, all order-dependent (or anisotropic) NMR interactions, (chemical shift anisotropy, dipolar and quadrupolar couplings) are no longer reduced to zero as in liquids. The residual value of these interactions (RCSA, RDC, RQC) can be then analytically exploited to investigate many molecular properties (dynamics, 3D structure, stereochemistry, isotopy, ...) [**27,28**].

In $^2H$-{$^1H$} NMR, the presence of the $^2H$ quadrupolar interaction modifies the Zeeman energy levels, thus leading to two transitions with distinct frequencies. Thus, in a homogenous and uniformly oriented LCs (uniaxial), the signal of a single $^2H$ nucleus ($I = 1$) becomes a symmetric quadrupolar doublet (QD) centred on $\delta^{aniso}(^2H)$ (with $\delta^{aniso}(^2H) \approx \delta^{iso}(^2H)$) where the separation (or splitting) between the two components (noted $\Delta\nu_Q$) is equal to the $^2H$-RQC value (see **Figure 2b**). In weakly aligning media (as polymeric LLCs), the EFG associated to C-$^2H$ internuclear directions is generally assumed to be axially symmetric along the $^{12,13}$C-$^2H$ vector (asymmetry parameter $\eta = 0$), and therefore $\Delta\nu_Q(^2H)$ can be simply expressed (in Hz) as a product of two terms, the quadrupolar coupling constant, (QCC or $C_Q$) and the local order parameter, $S_{C\text{-}2H}$ [**27,28,29,30**]:

$$\Delta\nu_{Qi} = \frac{3}{2} C_{Q_i} \times S_{C\text{-}^2H_i} = \frac{3}{2}\left(\frac{eQ_{D_i}V_{C\text{-}^2H_i}}{h}\right) \times \left(\frac{\left\langle 3\cos^2\left(\theta_{C\text{-}^2H_i}\right) - 1\right\rangle}{2}\right). \qquad (\mathbf{2})$$

In **Eq. 2**, $S_{C\text{-}^2H_i}$ and $\theta_{C\text{-}^2H_i}$ are the order parameter of the C-$^2H_i$ bond and the angle between the bond and the $B_o$ axis, respectively. Brackets <···> denote an ensemble average. Note here that the $C_Q$ value

POST-PRINT

varies approximately from 170 to 210 ± 5 kHz, depending on the hybridisation state of the bonded carbon atom as well as the electronic properties (+M, -I, …) of the adjacent substituents [**29,30**].

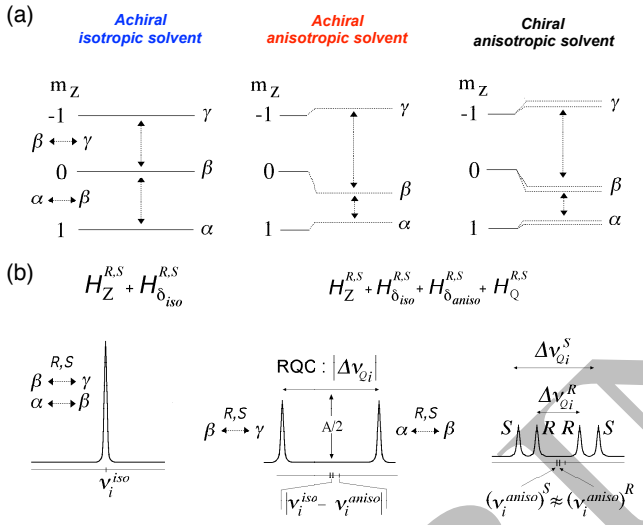


**Figure 2.** (a) Energy-level diagrams and (b) NAD-{$^1$H} 1D spectra expected for a pair of monodeuterated enantio-isotopomers dissolved in an achiral liquid (left), in an achiral liquid crystal (CLA) (middle) and in a CLC (right). The *R*/*S* assignment of QDs is arbitrary. Spectral patterns are plotted with the same vertical scale. Figure adapted from ref. **29** with permission.

From an analytical viewpoint, as the $^2$H singlets observed on isotropic NAD spectra are replaced by $^2$H-QDs, two $^2$H sites resonating fortuitous (no symmetry relationship) at identical chemical shifts can be differentiated on the basis of their $^2$H-RQC, which should not *a priori* be identical, since distinct C-D orientations are probed.

### *5.2 Recording NAD NMR spectra*

Unlike NMR of abundant nuclei, the absence of $^2$H-$^2$H coupling structures on the NAD-{$^1$H} spectra greatly simplifies their analysis [**28,29,30**], and this (current) non-detection of dideuterated isotopomers ($2.40 \times 10^{-2}$%) is an important advantage for measuring the $(^2H/^1H)_i$ ratios, both in isotropic and anisotropic media. In addition, even if the $^2$H quadrupolar interaction dominates the $^2$H relaxation mechanisms, the quadrupolar electrical moment of the deuterons, $Q_D$, (see **Eq. 2**) is low enough to prevent excessive line broadening [**30,31**]. Under these conditions, high-resolution $^2$H-{$^1$H} spectra are generally obtained, particularly when lyotropic LCs are used [**30**]. Nevertheless, it should be mentioned that the "disorder of order" of the mesophase can affect the linewidth of both components of QD, proportional to the magnitude of $^2$H-RQC [**31,32**].

POST-PRINT

The low value of the gyromagnetic ratio, $\gamma$, and the natural abundance of $^{2}H$ nuclei make basically NAD NMR much less sensitive than $^{1}H$ NMR [**30**]. Paradoxically, the first applications of this low-sensitive spectroscopy have been described since the 1970s in liquid phases, particularly with the arrival of the first commercially available Fourier transform NMR spectrometers [**33**]. In contrast, the first anisotropic NAD 1D spectra of analytes (and not the LC itself) were reported in the late 1990's both in thermotropic LCs (ZLI-1114) [**34**] and in polypeptide-based lyotropic CLCs [**35**].

Recently, the introduction of "high-field" NMR instruments with modern electronics (RF power capability, detection line, range of ADC, …) and $^{2}H$ cryogenic probes whose electronics (coil, condensators, preamplifier) are cooled with helium gas to limit the thermal noise, have considerably improved the sensitivity of NMR of low abundant/sensitive nuclei such as NAD NMR [**36**]. To set ideas, analytically exploitable NAD spectra can be recorded (with selective $^{2}H$ cryoprobe operating at 92 MHz (14.1 T)) in less than fifteen hours for analytes with a concentration in monodeuterated isotopomers in the order of 10 µmol/L. Clearly, the combined use of NMR spectrometers operating at very high-fields (> 23.5 T) and the latest generation of cryoprobes (manufactured by Bruker Biospin) should reduce the minimum detectable concentration by a factor of 1.5 - 2 in a near future.

Beyond the gain in sensitivity, the interest of working with very high-field spectrometers is also to improve spectral resolution, thus potentially facilitating the assignment of QDs according to their chemical shifts.

### *5.3 Spectral consequences of a chiral environment*

NMR spectroscopy has proven to be a powerful tool in the study of chiral and prochiral compounds when a chiral stimuli is used [**37,38,39,40**]. There are two types of spectral enantiodifferentiation. The first, referred to as enantiomeric discrimination, concerns the splitting of the NMR spectrum of racemates or other mixtures (scalemic) of optically active isomers, into NMR subspectra corresponding to each enantiomer [**41**]. The second type, referred to as enantiotopic discrimination, corresponds to spectral doubling signals resulting from the lifting of degeneracy of enantiotopic elements (atoms or directions) in prochiral molecules when dissolved in chiral solvents.

Due to the ability of CLCs to orient differently enantio-objects (molecules or directions), it becomes possible to spectrally differentiate the signals of enantiomers or enantiotopic directions. **Eq. 2** indicates that spectral $^{2}H$ enantiodiscrimination is detected when [**28,41**]:

$$\left| \Delta\nu_{Q_i}{}^{A} - \Delta\nu_{Q_i}{}^{B} \right| \neq 0 \qquad (\mathbf{3})$$

POST-PRINT

with subscripts *A*, *B* correspond to *R*/*S* or pro-*R*/pro-*S* classical stereodescriptors. In practice, the $^{2}$H-{$^{1}$H} spectrum of two monodeuterated "ordinary" enantiomers (i.e., chiral molecule of type (R,R′,R″)-C*D) dissolved in a CLC generally consists of two independent $^{2}$H-QD, one for each stereoisomer, centred approximately on the same chemical shift ($\delta^{aniso}(R) \approx \delta^{aniso}(S)$) (see **Figure 3c**). Discrimination also occurs when one of two QDs is equal to zero ($\Delta\nu_{Q_i} = 0$, $S_{C\text{-}D} = 0$) corresponding to the particular case where the angle $\theta_{C\text{-}D}$ is equal to the « famous » magic angle, $\theta_m = 54.7°$, (see **Eq. 2**) [**28**].

While the enantiomeric NMR discrimination in CLCs provides a robust alternative to classical isotropic NMR tools (using chiral derivatising agents (CDAs), chiral lanthanide shift reagents (CLSRs), chiral solvating agents (CSAs) [**37,38,39,40**], it is can be considered as a unique general approach for the discrimination of enantiotopic elements in prochiral compounds [**41,42,43**]. This capacity originates from the lowering of the "molecular" symmetry (defined as the effective symmetry as far as orientational ordering is concerned) which leads to the increase in the number of non-zero, independent order parameters for four symmetry molecular groups ($C_S$, $C_{2v}$, $D_{2d}$, $S_4$) [**44**]. For instance, five order parameters are necessary to describe the orientational behaviour of a $C_s$-symmetry, non-planar, rigid molecule dissolved in a CLC, in any initial axis systems (IAS), while only three are enough to do so in an ALC [**41,42,43**].

Doubling of signals observed on NAD NMR spectra can have two origins: (i) the chirality of the molecule (with or without stereogenic centre) observed on methyl, methylene or methine groups; (ii) the detection of isotopic enantiomers or enantio-isotopomers, (chiral isotopomers by virtue of the isotopic substitutions on $CH_2$ groups in prochiral molecules, (R-C*HD-R′). In case of $CH_2$ groups in a chiral molecule, we observe pairs of diastereo-isotopomers originating from the presence of two stereogenic centres in the corresponding monodeuterated isotopomers.

Finally note that the spectral discrimination of isotopic enantiomers originates from the fact that two enantiotopic directions (associated with the parent deuterated prochiral molecules (R-$CD_2$-R′) are already nonequivalent in CLCs [**41,42**]. This spectral nonequivalence allows us to distinguish the enantiotopic directions of hydrogenated prochiral (R-$CH_2$-R′) through their ANAD NMR spectrum [**41,43**].

Very intrigued by the analytical potential of NMR in polypeptide-based CLCs, Zeev Luz has actively collaborated in describing the phenomenon of enantiotopic discrimination in prochiral rigid or flexible molecules dissolved in these systems over the last decade [**45**]. As case study, he worked on the orientational behaviour of original analytes such as nonamethoxycyclotriveratrylene or hexathia metacyclopanes derivative [**45**] or naturally rare $S_4$-symmetry molecules such as icosane, a cyclic tetra-aza derivative, for instance [**46**]. From these experimental investigations, it has been demonstrated that

POST-PRINT

analysis of the enantiotopic discrimination in the NMR spectra of prochiral solutes embedded in CLCs could be achieved by symmetry factorisation of the Saupe order matrix where the equations for its non-zero elements factorise into two sets, termed as "symmetric" and "antisymmetric." Advantageously, this decomposition facilitates the analysis of spectra, and provides clearer insight on the discrimination mechanisms [**41,42**].

### *5.4 The QUOSY 2D experiments*

Unlike compounds regio- or enantioselectively enriched in deuterium, all monodeuterated isotopomers of a molecule are simultaneously detected by NAD NMR [**28,29,30**]. The ANAD spectra are therefore made up of a sum of independent $^2$H-QDs centred on different chemical shifts, the number of which depends on the number of inequivalent $^2$H sites of the molecule and the type of mesophase (chiral or achiral). Generally, the use of QUOSY-type (QUadrupole Order SpectroscopY) 2D experiments (*e.g.* mainly the *Q*-COSY Fz or *Q*-resolved Fz pulse NMR sequences) is necessary to separate the spectral information on two frequency domains ($F_1$ and $F_2$), to correlate the two components of each QD, and then to assignment them according their $^2$H chemical shifts [**47,48**]. It is, therefore, possible to decompose the NAD 2D maps into a series of NAD 1D subspectra associated with different enantio-/diastereo-isotopomers of the mixture. The schematic principle of this spectral decomposition in the case a *Q*-COSY-type experiment is illustrated in **Figure 3**. Note also that NAD QUOSY 3D experiments [**49**] as well as $^{13}$C-detection-based heteronuclear QUOSY 2D experiments (NASDAC NMR 2D sequence) have also been designed for spectral simplification purposes [**50**].

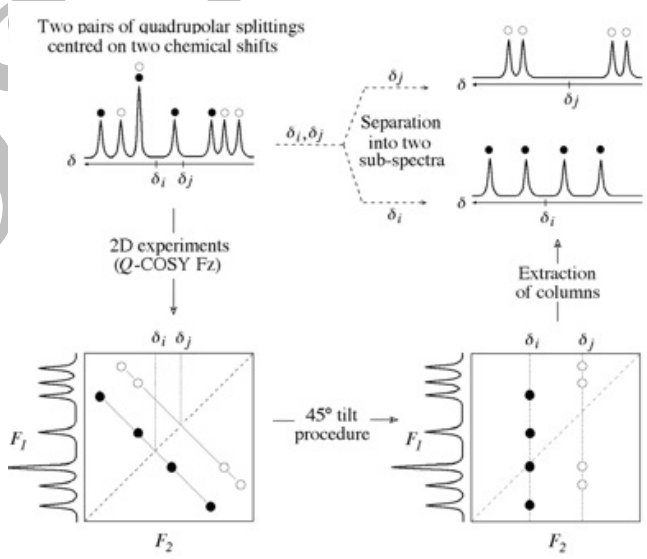


**Figure 3.** Schematic principle of editing each 1D subspectrum of a mixture of enantio-/diastereo-isotopomers by ANAD 2D-NMR. Here the case of *Q*-COSY-type 2D experiment is given. Figure adapted from ref. **30** with permission.

POST-PRINT

### *5.5 Helically-chiral-polymer based LLCs*

A vast arsenal of enantiodiscriminating lyotropic CLCs (based on organic co-solvents) has been developed over the past two decades. Among them, special attention was paid to chiral LLCs based on helically-chiral-polymer, such polypeptide-based homopolymers with different achiral side chains as PBLG (see **Figure 4a**), PCBLL, PELG, … or their mixtures, for several reasons [**51,52**]: (i) their commercial availability with a large range of degree of polymerization (DP); (ii) a vast choice of compatible organic co-solvents, from polar (as Pyridine (Py), DMF, TMU) to weakly polar (as $CH_2Cl_2$, $CHCl_3$); (iii) a rather simple preparation of samples. In this context, the PBLG enantiodiscrimination efficiency has been established for almost all classes of organic chiral molecules, but also for other aspects of the enantiomorphism, such as chirality by virtue of the isotopic (D/H) substitution, or the enantiotopy in prochiral molecules [**41, 42,53**].

Since a few years, new enantiodiscriminating helically chiral polymeric LLCs made of polyguanidines [**54**], polyisocyanopeptides [**55**], polyarylisocyanides [**56**] or polyacetylenes (PLA) [**32,57**] with chiral side chains (**Figure 4b**) were reported in literature. For this latter, significant ANAD NMR results were obtained in 2018, in particular with flexible, chiral alkanes [**32**]. For the investigation of fatty acids and related compounds described here, only PBLG-based chiral phases have been used and optimised.

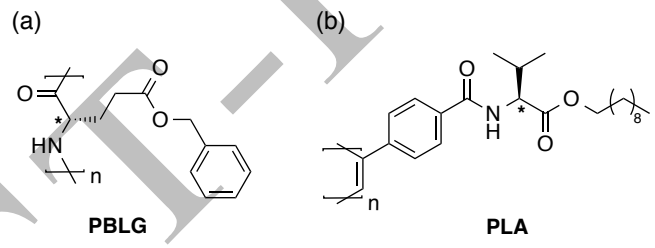


**Figure 4.** Structures of (a) PBLG and (b) *L*-valine-derived PLA homochiral polymers. Note the difference of positioning of the stereogenic centre (backbone *versus* side chain).

## 6. The fatty acids (FA) family

Supplied by food, fatty acids (FAs) are important family of organic compounds, classified within the lipid macronutrient class. They are source of carbon atoms and energy (fuel) in most animals, and to a lesser extent in plants, stored as triglycerides, and for some of them (called essential fatty acids) are involved in many biological processes in human metabolism. They also play an important role in the formation of cell membranes (as a component of phospholipids and glycolipids), giving them particular physical and mechanical properties (elasticity, flexibility) [**58,59**].

Structurally, FAs are lipidic carboxilic acid with an hydrophilic polar head and hydrophobic, (unbranched) aliphatic chain which is either saturated or unsaturated, with an even number of carbon

POST-PRINT

atoms (from 4 to 28) [**60**]. They are also characterised by the number and type of unsaturation (double or triple bond), their stereochemistry (*Z* or *E*) and their respective position in the unsaturated lipid chain. Depending on the position of the last unsaturation, they are called ω-3, ω-6, ω-9, ... (see **Figure 5**). Three classes of FAs can be defined: i) saturated fatty acids (SFAs); ii) mono or polyunsaturated fatty acids (PUFAs); (iii) conjugated unsaturated fatty acids(CUFAs). The main FAs present in seed oils of most plants have a chain length of 16 or 18 carbon atoms and between zero and three double bonds of *Z* configuration [**60**].

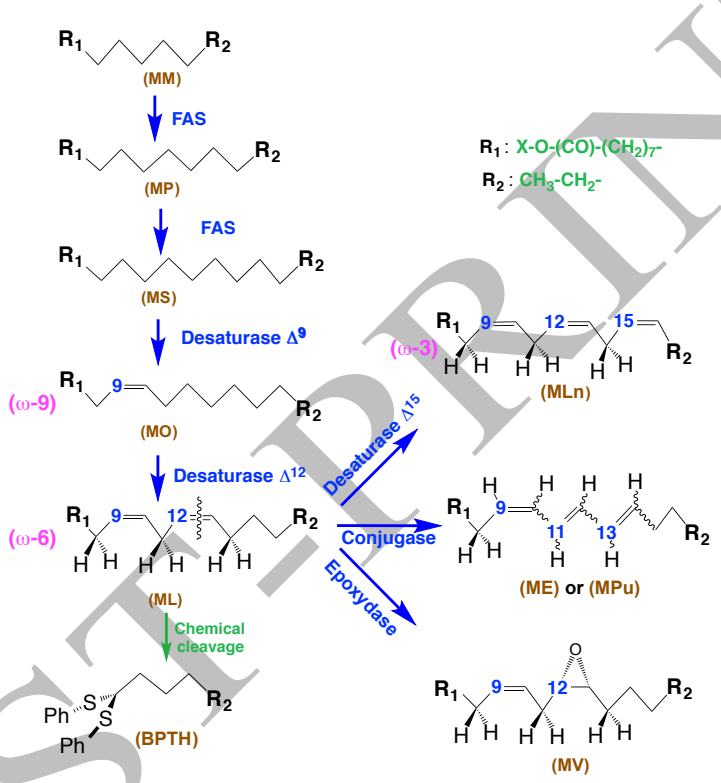


**Figure 5.** Scheme of successive biochemical transformations of methyl myristate (**MM**), (C-12 SFA) leading successively to longer SFAs (C-16 and C-18), methyl palmitate (**MP**) and methyl stearate (**MS**), and then to UFAs, (9*Z*)-**MO**, (9*Z*, 12*Z*)-**ML**, (9*Z*, 12*Z*, 15*Z*)-**MLn**, (9*Z*, 12*R*, 13*S*)-**MV** or two CUFAs, (9*Z*, 11*E*, 13*E*)-**ME** and (9*Z*, 11*E*, 13*Z*)-**MP**. In plant or microorganism cells, X corresponds to coenzyme A (CoA) or carrier protein (ACP). For NAD NMR analysis, X is a methyl group.

From acetyl-coA, FAs are biosynthesised by the enzyme "Fatty Acid Synthesase" (FAS) by a replication mechanism, then modified under the action of different enzymes (Conjugase, Desaturase, Epoxydase). To simply illustrate the purpose, **Figure 5** presents the successive transformations of methyl stearate (**MS**), a C-18 saturated AG into methyl oleate (**MO**, 9*Z*-18:1), methyl linoleate (**ML**, 9*Z*, 10*Z*-18:2), and then in a second step of enzymatic reactions into methyl linolate (**LnM**, 9*Z*, 12*Z*, 15*Z*-18:3), methyl *α*-eleostearate (**ME**, 9*Z*, 11*E*, 13*E*,-18:3) or methyl punicate (**MPu**, 9*Z*, 11*E*, 13*Z*-18:3)) and methyl vernoleate (**MV,** 9*Z*, 12*R*, 13*S*,-18:1), from the **ML**. Among PUFAs investigated,

POST-PRINT

only **MV** possess stereogenic centres (sites 12 and 13) which the stereochemistry is known (12*R*,*13S*). **MV** is mainly used in paint industry. Finally, the 1,1'-bis(phenylthio)hexane (**BPTH**) is a fragment of **ML** obtained by chemical cleavage (see below). **ML** and **MLn** are termed as essential FAs.

For simplicity, it will refer indistinctly to FAs or fatty acid methyl esters (FAMEs) obtained after esterification, but all (A)NAD NMR analyses have been performed with FAMEs.

## 7. Proof of concept

### *7.1 From ML to BPTH*

Derived from **MS**, the **ML** is a central PUFA which is the precursor of many others FAs (see **Figure 5**). The complete determination of its isotopic fractionation by measuring of ($^2$H/$^1$H) ratios on all its hydrogenated sites is therefore a major challenge to clarify certain aspects of the bioenzymatic mechanisms (stereochemical aspects) leading to its formation or to understand its transformation into CUFAs or other derivatives. As seen in **Figure 6a**, **ML** is a prochiral, flexible molecule of $C_s$ symmetry in average, according to the Altman's definition (so important for Zeev Luz) [**61**]. Even recorded at high field, the SNIF-NMR™ spectra of **ML** shown that only 30% of $^2$H signals are detectable (*i.e.* 8 sites on the 26 possible unequivalent sites) (see **Figure 6b**) [**62**].

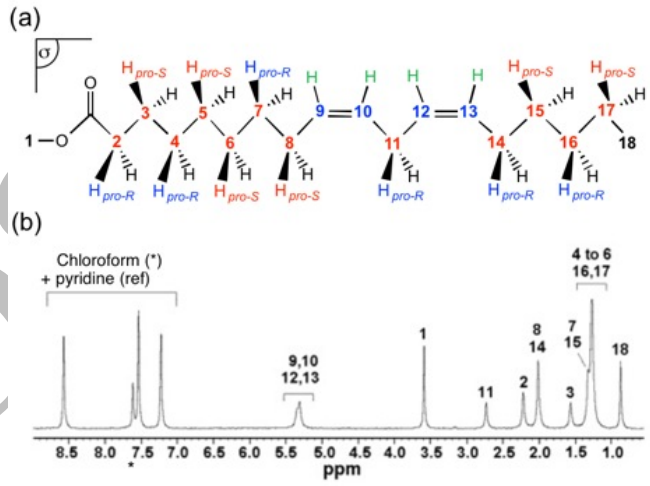


**Figure 6.** Structure along with the numbering and the stereochemical description of the **ML** according to CIP rules. Here, only the stereodescriptors of the hydrogen atoms in front of the plane of symmetry are presented. (b) SNIF-NMR™ spectrum (92.1 MHz) of **ML** at 310 K. Figure adapted from ref. **62** (Supp. Info) with permission.

In an attempt to overcome this inappropriate situation, it was demonstrated in 2001 the possibility of cutting (three chemical steps) the **ML** (at the second double bond) into three fragments, one of which is

PCCP PRINT

the **BPTH** (see **Figure 3**), to simpler determine the isotopic ratios of sites 14 to 18 [**25,26**]. Unfortunately, despite the reduction of the alkyl chain length to four methylene groups and the presence of thiophenyl groups to increase the chemical dispersion of $^2$H signals, the isotropic SNIF-NMR® spectrum of **BPTH** shows that methylene sites 4 and 5 are not resolved even at 11.7 T or over (14.1 T). This fortuitous pseudo-isochrony was first left by recording the anisotropic NAD spectra of **BPTH** using a polypeptide-based achiral LC made of a racemic mixture of PBLG and its enantiomers (PBDG) [**26**]. In this compensated mixture (noted PBG), two enantiomers (or enantiotopic directions) are in rapid exchange between the two polypeptide helices of inverted configuration (*L* and D), resulting in the elimination of all enantiodiscriminations on average [**63**]. The same situation can be also obtained in case of racemic mixture of *L*/*D*-valine derived polyacetylene helices [**32**]. As seen in **Figure 7b**, the two methylene sites are discriminated on the basis of their respective $^2$H-RQCs (two QDs). In a second step, the discrimination of monodeuterated enantio-isotopomers on the NAD NMR spectra, and hence the measurement of isotopic ratios for each enantiotopic hydrogenated site is possible by using a single polymer (PBLG or PBDG), the LC becoming chiral (see **Figure 7c**). It is also interesting to note that replacing the PBLG with the PBDG simply verifies whether the difference in peak intensity observed for pairs of enantio-isotopomers is due to a variation in ratios ($^2$H/$^1$H) and not to another unwanted effect. frame of isotopic investigation as a complement tool or as an alternative to the historical approach [**26**].

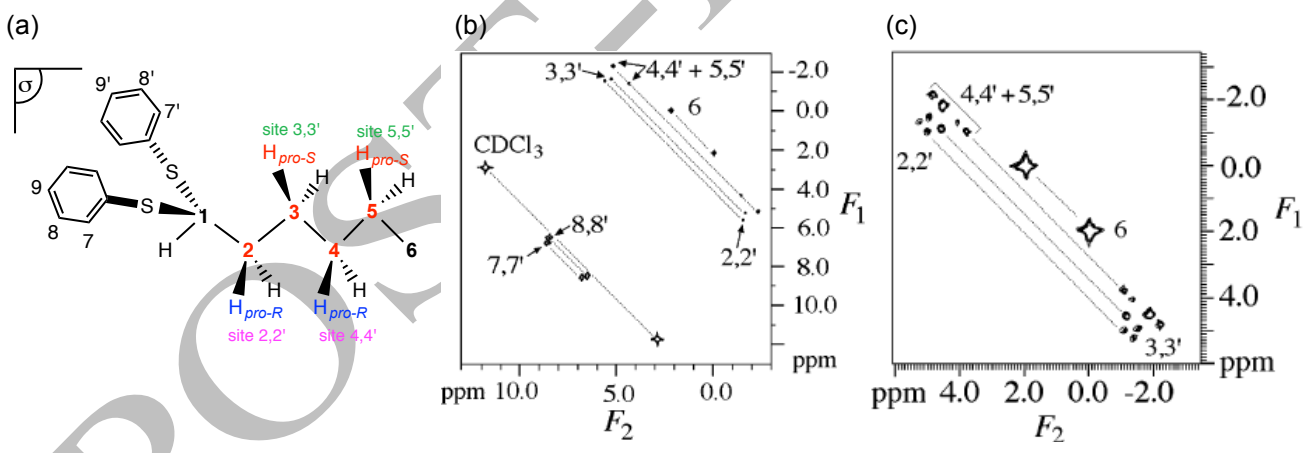


**Figure 7.** (a) Chemical structure of **BPTH** along with the atomic numbering. No stereochemistry is defined here. (b) NAD-{$^1$H} *Q*-COSY 2D spectrum (magnitude mode) of **BPTH** in the PBG/$CHCl_3$ achiral phase. (c) Aliphatic region of NAD-{$^1$H} *Q*-COSY 2D spectrum of **BPTH** in the PBLG/$CHCl_3$ chiral phase showing four QDs for the sites 4/4' and 5/5'. ANAD 2D spectra were recorded at 61.4 MHz (9.4 T) within a night. Figure adapted from ref. **26** with permission.

Indeed, the chirality of PBDG helices compared to PBLG ones is reversed, and therefore the direction of the potential interaction is opposite to that of PBLG. As a direct result, the $^2$H-QDs associated with the orientation of (*S*)-enantiomeric isotopomers in the PBLG now correspond to the QDs of (*R*) enantiomeric

POST-PRINT

isotopomers in the PBDG phase and *vice versa* [**62**]. The overall experimental results obtained with **BPTH** have revealed that the variation of isotopic ratios (enrichment/depletion) for odd and even $CH_2$ groups, thus confirming previous conclusions, as well as the significative variations of isotopic ratios at enantiotopic positions, thus establishing for the first time the potential of anisotropic NAD NMR in the

### *7.2 Assignment of stereodescriptors in ANAD spectra*

The assignment of the absolute configuration (AC) for the two QDs associated to an enantio-isotopomer pair) is a challenging task and a long-standing problem for small chiral molecules with a single stereogenic centre [**64**]. Same difficulties also exist for the assignment of enantiotopic elements in prochiral molecules. Indeed, there is not a direct correlation between the AC and the magnitude of $^2$H-RQCs for two monodeuterated enantiomers or dideuterated enantiotopic directions. AC assignment by comparison with parents [**65**] or reference or analoguous references has been however been proposed [**66**].

To investigate further the origin of depletion/enrichment effects observed in enantiotopic positions in methylenes 4 and 5, the assignment of QDs must be determined. In practice, the assignment of *R*- and *S*-isomers was deduced from the (D/H) isotopic substitution in positions 4/4' and 5/5' in the aliphatic chain of **BTPH** derived from its precursor natural (linoleic acid), using an optimised chemical strategy to synthesize separately four regio- and stereoselectively monodeuterated enantiomers of **BTPH**. By reference to the $^2$H-{$^1$H} spectra in PBLG CLC of these isotopically labeled reference compounds, it has demonstrated that, on both methylene groups 4 and 5, the enantio-isotopomer of (*S*)-configuration is isotopically depleted relative to those of (*R*)-configuration [**26,67**]. Actually, it is possible to assign the QDs to enantiomeric monodeuterated isotopomers at methylene groups in **ML** on the basis of the stereochemical assignments made of **BPTH**, and the mechanism of stearoyl biosynthesis (see **Section 8.4**).

## 8. Analysis of four unsaturated FAMES

### *8.1 OM, ML, MLn and MV*

The pioneering results obtained with **BPTH** have really paved the way for exciting analytical challenges, such as the NMR study of C-18 PUFAs and CUFAs. To this end, the use of new phased-type QUOSY 2D experiments [**48**] and a 14.1-T NMR spectrometer equipped with a selective $^2$H cryoprobe to benefit from greater sensitivity and better resolution have been combined to study four complete unsaturated FAs, **MO**, **ML**, **MLn** and **MV** (see **Figure 5**) [**62**]. Compared to the

POST-PRINT

technological/methodological employed for the **BPTH** study (9.4 T, standard probe, magnitude mode experiments), this new combination allowed a significant gain in sensitivity of between 7 and 8.

For this first new series of FAs, the experimental NAD NMR results obtained in PBLG/chloroform phase have shown that about 90% of theoretically inequivalent $^2$H sites in a CLC could be discriminated. The results have therefore demonstrated a significant progress in measuring the natural $^2$H fractionation of UFAs, and how unique information inaccessible by isotropic classical tools can be effectively revealed with three significant advantages: (i) removing the risk to introducing non-natural $^2$H fractionation during the chemical modification; (ii) greatly reducing the time spent in sample preparation (no chemistry); i(ii) access to isotopic ratios of almost all enantiotopic sites for the first time; iv) access to ethylenic fragment, and the associated ratios. These two last advantages are illustrated in **Figure 8** where the ethylenic parts and the adjacent methylene sites of **MLn** are observed simultaneously [**62**].

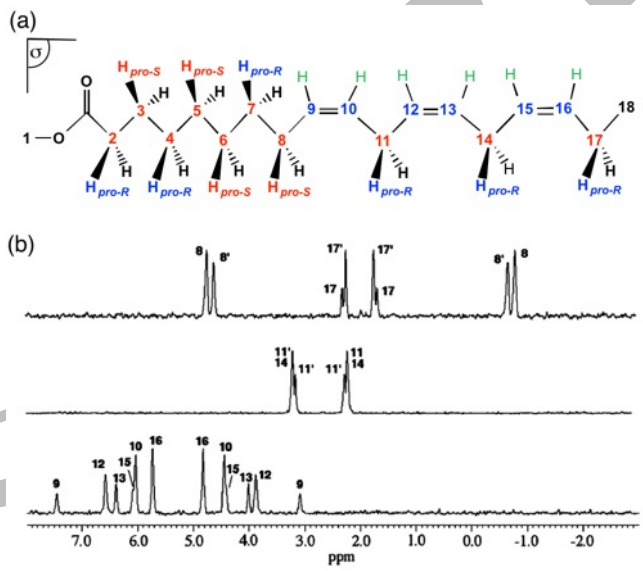


**Figure 8.** Three $^2$H-{$^1$H} 1D subspectra extracted from the NAD 2D map of **MLn** in PBLG/$CHCl_3$. Figure adapted from ref. **62** with permission.

### *8.2 Orientational and conformational behaviour*

Beyond the isotopic data analysis, the orientational/conformational behaviour of these four UFAs was investigated. To this end, the variation of the average of $|\Delta\nu_Q$'s$|$ measured in PBLG/$CHCl_3$ along the chain (see **Figure 9**) was examined with the aim to understand the effects of double bond(s) and epoxyde ring on the orientational mechanisms, and so get insights on their alignment within the polymeric phase. Interestingly, the analysis of RQC data have highlighted that: (i) the four UFAs behave quite identically, (ii) they possess two independent flexible molecular fragments ($C_2$-$C_8$ and $C_{11,14,17}$-$C_{18}$) separated by a

"pseudo rigid" linker ($C_9$-$C_{13}$) created by the double bond(s) in **MO**, **ML** and **MLn** and the double bond and the epoxide ring in **MV**, iii) the presence of linkers decorrelate the orientational behaviour of the two parts, generating a discontinuity along the chains compared to SFAs (see **Section 10.2** and **Figure 17**), the effect being much less marked for **MO**.

These results have been confirmed by simple molecular modelling (MM) calculations using a semi-empirical method (AM1) [**62**]. Thus, it was established that the structure of the $C_2$-$C_8$ fragment (characterised by seven $CH_2$ rotors) for the lowest energy conformer was superimposable for all molecules, leading to reasonably assume that the conformational dynamics of the first fragment is very similar for all UFAs, both in the gas phase and in oriented solvent. In contrast, even if their molecular long axis are oriented more or less parallel along the PBLG fibres, the degree of bending due to the number of rigid linkers differently affects the orientation of the second fragment ($C_{11,14,17}$ –mes re $C_{18}$) in the four molecules; the most bent molecule (« hairpin » conformation) being the **MLn**. This situation leads to large variability in the magnitudes of $^2$H-RQCs for terminal sites compared to **MS**.

### *8.3 Enantiodiscrimination optimisation for ML*

In case of **ML**, the enantio-isotopomers associated to methylene 11 group (see **Figure 6**) have been not differentiated using $CHCl_3$ as organic co-solvent [**62**]. Various experimental parameters (temperature, sample composition, nature of polymer, polarity of co-solvent) can be modified to modulate the enantiodiscrimination mechanisms in polypeptide LLCs, thus improving the number and differentiation magnitude of enantio-isotopomers. Experimental investigations have shown that the first two factors mentioned above had a limited influence for **ML**, but the polarity of helicogenic organic co-solvent induced significant effects on the enantiodiscrimination mechanisms. The analysis of results involving four organic solvents with polarity varying between 1.04 and 3.85 D revealed that PBLG/Py provided better results, including the enantiodifferentiation at site 11 (see **Figure 10**).

While the role of co-solvent polarity in orientation mechanisms is not yet fully understood, the observed trend clearly shows that intermolecular potentials depend on the dielectric constants of their environments [**68**]. Finally, it should be noted that TMU can provide an attractive alternative to pyridine, with the advantage of being also usable as an internal isotopic reference for absolute quantification measurements.

**Figure 11** presents the series of ANAD 1D subspectra (extracted from the tilted *Q*-COSY Fz map recorded at 305 K) of **ML** dissolved in the PBLG/Py phase. As seen, the NAD signals of all inequivalent isotopomers are visible and resolved [**69**], thus permitting to access (for the first time) the measurement of isotope ratios $(^2H/^1H)_i$ at all ethylenic positions and all enantiotopic pairs in the chain.

POST-PRINT

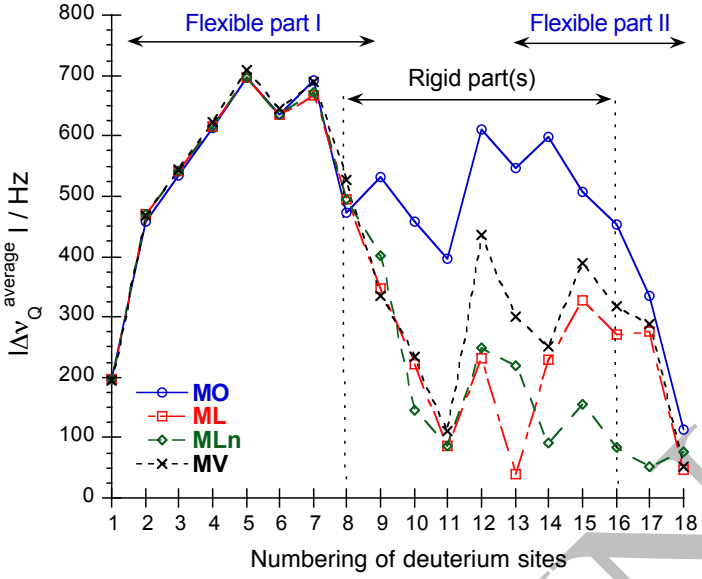


**Figure 9.** (a) Comparison of the average of $|\Delta\nu_{Q's}|$ of **MO**, **ML**, **MLn** and **MV** dissolved in PBLG/$CHCl_3$ *versus* the $^2H$ sites at same T (300 K). Figure adapted from ref. **62** with permission.

### *8.4 Analysis of isotopic profile of ML*

As ANAD spectra were recorded using quantitative conditions, the variations in $^2H$-QD intensity observed on the NAD subspectra show the effects of enrichment or depletion in $^2H$ for all sites of the molecule, but a (statistical) measurement of the peak area is necessary to properly determine the complete isotopic profile.

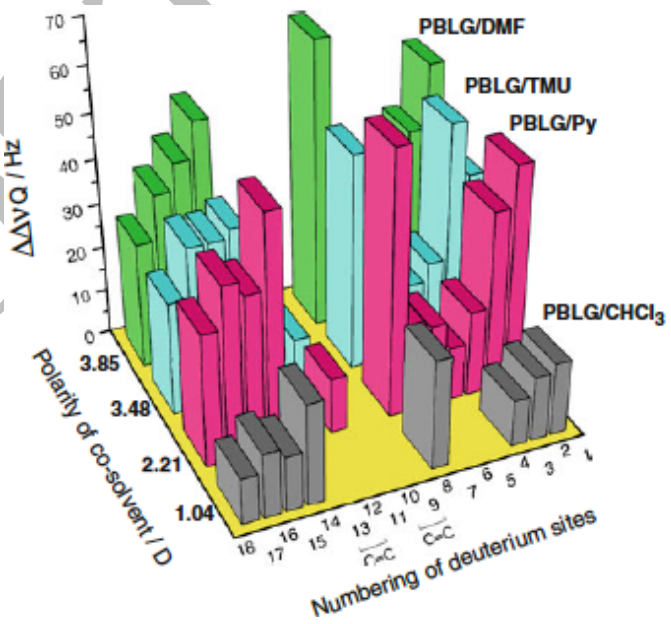


**Figure 10.** Comparison of the difference (stack plot) of RQC s for **ML** oriented in the four mesophases *versus* the $^2H$ site In this 3D stack plot, the columns are ranked from the highest (top) to lowest (bottom) polarity co-solvents. Figure adapted from ref. **68** with permission.

POST-PRINT

Since no internal chemical reference was added in the anisotropic sample, the absolute ratios $(^2H/^1H)_i$ measured on this spectrum have been calculated from the ratios $(^2H/^1H)$ determined by isotropic, quantitative NAD 1D-NMR according to **Eq. 4** [**62,69**],

$$\left(\frac{^2H}{^1H}\right)_i^{aniso} = \frac{(S_i\ \%)}{100} \times n \times \left(\frac{^2H}{^1H}\right)_i^{iso} \qquad (\mathbf{4})$$

where n is the number of equivalent deuterium atoms contributing to the isotropic NAD signal. This two-step approach is only valid if the source of the analyte studied is identical in both samples. The graph in **Figure 12a** shows the variation of $(^2H/^1H)$ isotopic ratios of methylene groups along the chain. As we can see the $(^2H/^1H)$ ratios value differ significantly from the V-SMOW value and the differences in values for enantiotopic sites (of the same $CH_2$ group) vary between 10 ppm (site 2) and 91 ppm (site 15). This strong depletion at the pro-*R* enantiotopic site of methylene 15 had also been

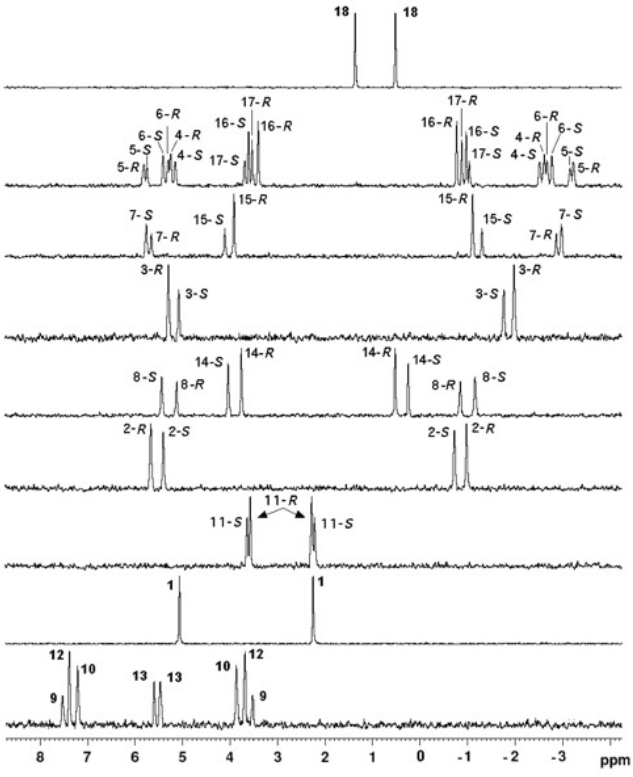


**Figure 11.** Series of NAD-{$^1$H} 1D subspectra data extracted from the tilted *Q*-COSY Fz map (92.1 MHz) of **ML**, and recorded under quantitative conditions in the PBLG/Py phase at 310 K. See the molecular structure of ML in Figure 6(a) for the peak numberingFigure adapted from **69** with permission.

observed at the corresponding site in **BPTH** (position 4) obtained from **ML** by chemical cleavage. Finally, it should be noted that the enrichment/depletion effect in $^2H$ at even/odd methylene sites along the chain, initially demonstrated by isotropic NAD NMR, was also found on ANAD spectra. In addition

POSTPRINT

to the absolute measurement of ratios ($^2H/^1H$), it is now possible to evaluate the value of the enantio-isotopomeric excess (*eie*) for each $CH_2$ group along the chain according to **Eq. 5** [**69**]:

$$eie_i = 2\times\left|\frac{\left(\frac{^2H}{^1H}\right)_i^{pro-R}-\left(\frac{^2H}{^1H}\right)_i^{pro-S}}{\left(\frac{^2H}{^1H}\right)_i^{pro-R}+\left(\frac{^2H}{^1H}\right)_i^{pro-S}}\right| \quad (\mathbf{5})$$

The variations of the *eie's* for the **ML** are presented in **Figure 12b**. In this example, we show that the *eie's* are larger for the odd $CH_2$ in the chain. This trend is due to the difference in the mechanisms of incorporation of hydrogen atoms during the elongation process of FAs (via the **FAS** enzymatic complex) [**67**]. In fact, in odd sites, hydrogen is incorporated by the action of two different reductases using NAD(P)H/$H^+$ as co-factor, while in even $CH_2$ groups the two hydrogen atoms are mainly provided by the cell water (in exchange), and to a lesser extent by sodium acetate [**70**]. With the exception of site 2, the *eie*'s on even sites remain practically unchanged at about 10 ± 2% throughout the chain. The lowest value for site 2 is probably associated with a higher exchange effect given the higher acidity of the hydrogen adjacent to the carbonyl group.

The stereodescriptors, *R*/*S*, for the assignment of QDs on the NAD 1D subspectra ol **ML** in **Figure 11** and **Figure 12** are associated with each pair of enantio-isotopomers in the mixture (corresponding to the pairs of pro-*R*/pro-*S* enantiotopic hydrogenated sites in the molecule. The AC assignment of QDs is not direct and has been carried out according to the following criteria: i) since the two analytes have the same botanical origin (Carthamus tinctorius), the stereochemical assignment of the $^2H$-QD associated with methylenes 4 and 5 of **BPTH** (fragment of the **ML**) is identical to that of sites 16 and 17 of **ML** (cf. **Figure 5**); ii) the elongation of the FA chain leading to the saturated precursor (**MS**) always follows the same process (addition of two carbons from acetate in each cycle of the Fatty Acid Synthetase (**FAS**) activity, the origin and prochirality of hydrogen at each type of methylene site (odd or even) is the same [**26**], and hence the trend observed for **BPTH**, namely that the ratios ($^2H/^1H$) are always smaller for pro-*S* positions both for even and odd $CH_2$ groups (from 15 to 2) can be applied in the case of **MS**, precursor of **ML**. Formally, this second argument is only valid for the **MS** because the stereodescriptors associated with the $^2H$ positions located in front of the molecular symmetry plane (see **Figure 15a**) are always the same along the chain, according to the Cahn-Ingold & Prelog (CIP) rules. For the **ML**, this stereochemical assignment in accordance with CIP priority characteristic is only partially true since for the methylenes 6, 7 and 8, the stereochemistry of the $^2H$ sites located in front of the plane of symmetry is reversed due to the presence of the double bond in position 9-10 (see **Figure 6**) [**71**]. With the exception of sites 6 to 8, stereodescriptors (*R*/*S*) were therefore assigned to the most intense QD on the NAD 1D subspectra.

POST-PRINT

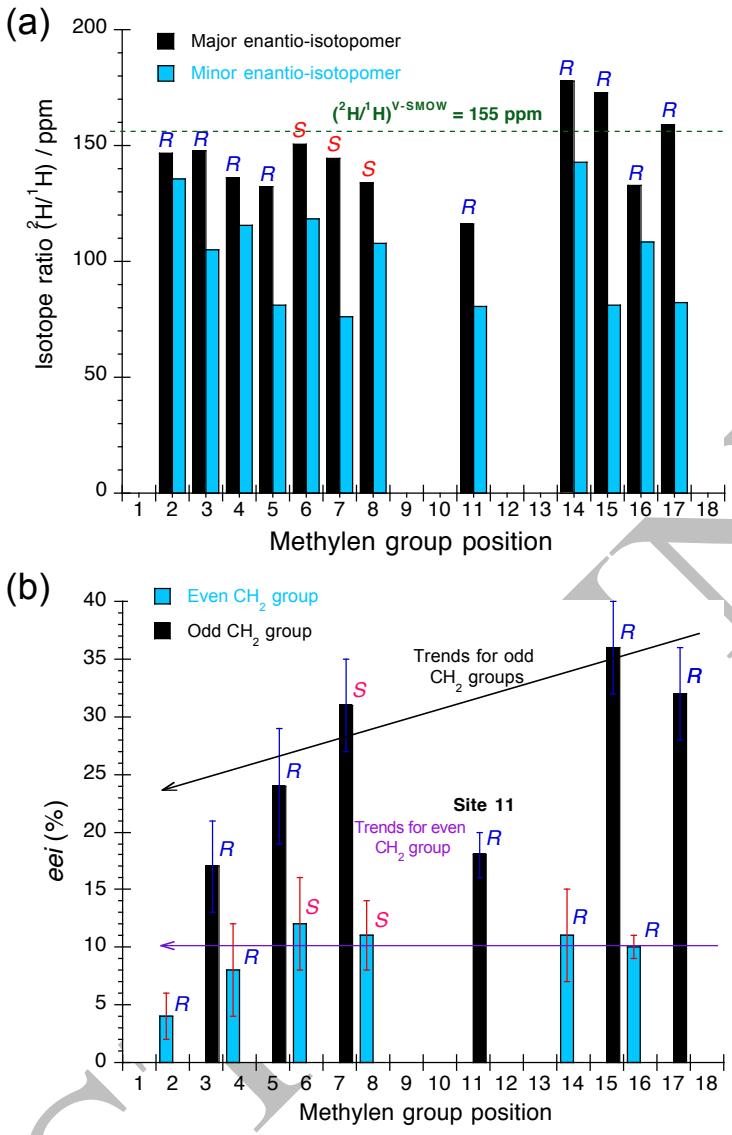


**Figure. 12**. (a) Variation of the $(^2H/^1H)_i$ isotope ratios along the **ML** chain. (b) Variation of *eie's* for each methylene. The absolute configuration given corresponds to the enantio-isotopomer most naturally enriched in $^2H$ (in accordance with CIP rules). Figure partly adapted from ref. **69** with permission.

## 9. Conjugated unsaturated FAs

To further explore the potential of the ANAD 2D NMR in the field of enzymatic mechanism studies, in a third step, the approach was applied to analyse two conjugated UFAs such as (9*Z*, 11*E*, 13*E*-18:3)-**ME** and (9*Z*, 11*E*, 13*Z*-18:3)-**MPu**), two prochiral isomers of **MLn** [**68**]. These two CUFAs, obtained by action of (1,4)-acyl-lipid-desaturases or, more commonly called conjugases, on **ML** (see **Figure 5**), potentially possess antitumoural activities or cancer-cell inhibition activities.

To obtain key information on the enzymatic mechanism leading to these conjugated triene system from **ML**, access to $(^2H/^1H)_i$ isotope ratios at the six ethylenic positions is crucial; specifically

POST PRINT

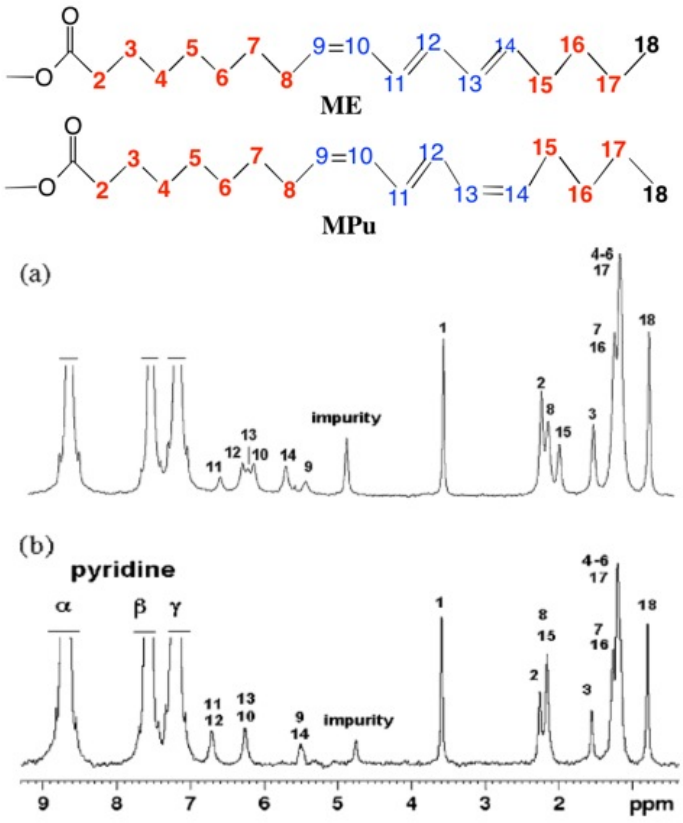


**Figure 13.** Isotopic NAD-{$^1$H} 1D spectra of (a) (9*Z*, 11*E*, 13*E*)-**ME** and (b) (9*Z*, 11*E*, 13*Z*)-**MPu**. Figure adapted from ref. **68** with permission.

to establish: i) which hydrogen (pro-*R* or pro-*S*) is eliminated from **ML**; ii) which position is submitted to a $^2$H KIE to point out which C–H cleavage is the limiting step in the (1,4)-elimination reaction [**68,72**].

Based on the ANAD results for **ML**, pyridine was selected as polar co-organic solvent both for recording isotropic and anisotropic NAD NMR. **Figure 13** presents the isotropic NAD 1D spectra of **ME** and **MPu** where important variations of $^2$H chemical shifts (sites 8 - 15) due to the difference in the double bonds configuration (*Z*,*E*) are observed. As already seen for **ML** in $CHCl_3$ (see **Figure 7**), important sites (8, 10, 12, 13 and 15) are poorly resolved.

Replacing pyridine by the mesophase PBLG/Py has improved the situation. For illustrating the discussion, the series of NAD 1D subspectra extracted from tilted *Q*-COSY Fz map of **ME** is given in **Figure 14**. Thus about 90% of all $^2$H sites are now discriminated instead of 40 % on the isotropic spectrum. Globally, the experimental results indicated the possibility to access to the important $^2$H sites of **ME** and **MPu**. Surprisingly, the ethylenic sites showed very small S/N ratios (5 to 9) for both CUFAs. Actually, such a situation can originate from: (i) an unusual strong impoverishment of $^2$H for the sites; (ii) longer $T_1(^2H)$ values in regard of the recycling time of the 2D experiments used; (iii) a significant line broadening due to small $T_2(^2H)$ values; iv) a combination of these various effects.

POST-PRINT

## 10. The difficult case of saturated fatty acids

Saturated fatty acids (SFAs) are the precursors of unsaturated FAs. Three of them, methyl myristate (**MM**, C-14), methyl palmitate (**MP**, C-16) and methyl stearated (**MS**, C-18) have been explored by ANAD 2D NMR (see **Figure 5**).

Compared to UFAs, the NAD NMR analysis of SFAs with long chain (C-14 to C-18) presents two additional difficulties compared to UFAs. First, the absence of double bonds or other groups in the centre of the chain that considerably reduces the dispersion of the $^2$H chemical shifts of methylene groups. Typically, the isotropic NAD 1D spectrum of the **MS** shows a single broad resonance (at ≈ 1 ppm) corresponding to the sum of all $^2$H signals from the methylene positions 4 to 17 (see **Figure 15b**), but same situation occurs for **MM** and **MP** [**73**]. For instance, for **MS**, only 27% of all possible inequivalent $^2$H sites are resolved when recording the NAD spectra at 14.1 T in an achiral liquid phase (pyridine). Given the significative pseudo-isochrony of these sites, the resolution of the $^2$H signals cannot be reached whatever the strength of the magnetic field [**73**]. Second, SFAs cannot be simply chemically cleaved into smaller fragments to reduce the $^2$H signal overlapping. Under these conditions, the ANAD 2D-NMR becomes the (current) last tools for potentially maximasing the number of $^2$H sites detected, and then investigating their site-specific isotopic profile.

Analysis of ANAD results in the PBLG/Py chiral phase showed a significant increasing of $^2$H sites discriminated (theoretically inequivalent in a CLC) compared to isotropic spectra. However, this number decreases when the chain length and consequently the number of methylene groups increases (from C-14 to C-18), with 66% of $^2$H sites for **MS** (value to compared to one recorded in liquids). For all SFAs, enantiodiscrimination was particularly visible at methylene sites at the sides of the chain, particularly at positions 2 and 3 (not shown) or 16 and 17.

Smaller discrimination was obtained for the other methylene groups as we can see in **Figure 16a** which zooms on the aliphatic region of NAD 2D spectra of **MS**. As previously, the difference in intensity (surface area) between the QDs associated with pro-*R*/pro-*S*enantiotopic pairs is due to natural isotope fractionation. A very strong difference in deuterium enrichment/depletion can be observed on the enantiotopic directions of the methylenes 16 and 17. This situation is found on the same sites of the **ML**, which is successively biosynthetised from the **MS** *via* the **MO**. The similarity of the isotopic profile at the terminal methylene sites of the three FAs is not *a priori* surprising since the desaturases $\Delta^9$ and $\Delta^{12}$ (see **Figure 5**) essentially affect the isotopic fractionation of the methylene groups (at positions 9 and 12) oxidised by these enzymes and adjacent sites. Therefore, the ratios $(^2H/^1H)_i$ of $CH_2$ groups distant from double bonds are expected to very similar to those measured on successive precursors.

POST-PRINT

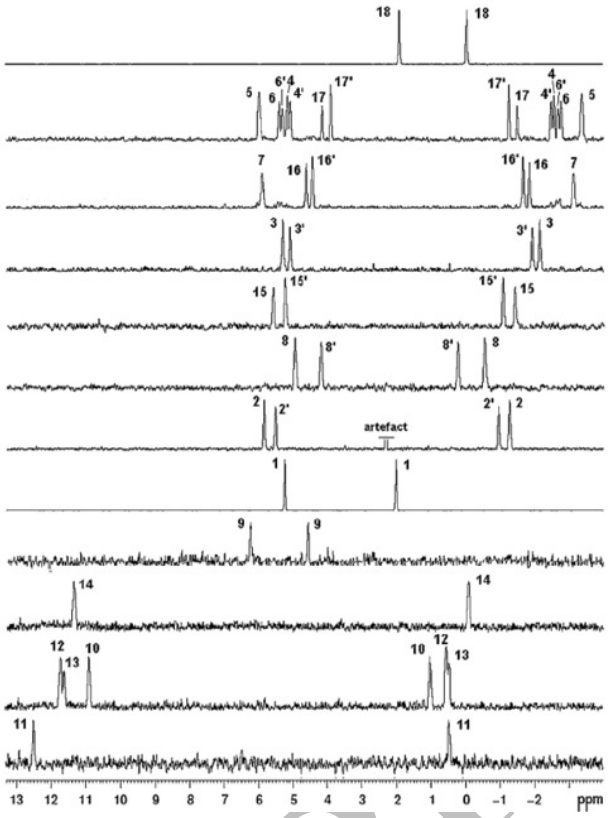


**Figure 14.** Series of NAD-{$^{1}$H} 1D subspectra extracted from tilted *Q*-COSY Fz map of **ME** (92.1 MHz) in PBLG/Py phase. See the molecular structure of **ME** in Figure 13 (top) for the peak numbering. Figure adapted from ref. **68** with permission.

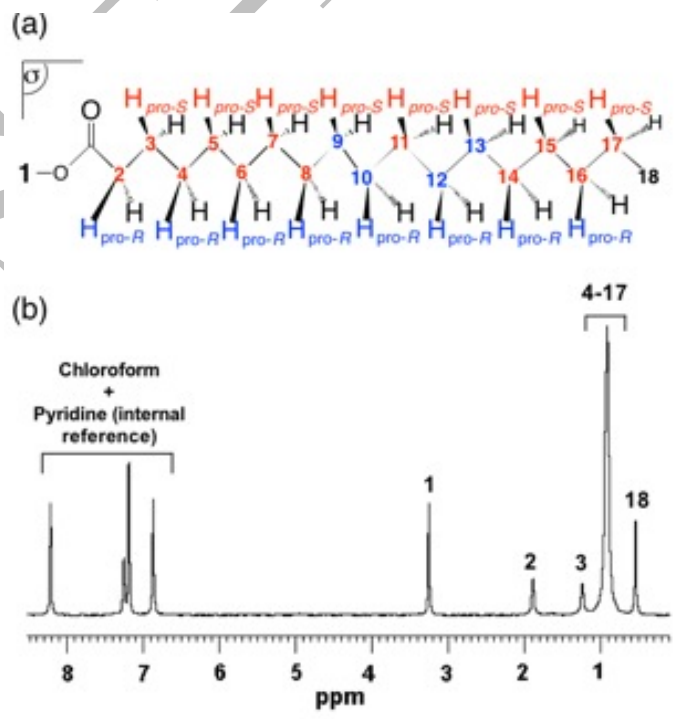


**Figure 15.** (a) Structure, atomic numbering and stereodescriptors (*R*/*S*) of the MS. (b) Isotropic NAD 1D spectrum SNIF-NMR$^{TM}$ (92.1 MHz) at 310 K. Figure adapted from ref. **73** with permission.

POST-PRINT

### *10.1 Assignment of central methylene groups*

So far, the assignment of $^2$H-QDs associated to central methylene groups in FAs was made from different sources of information such as the variation of chemical shift values, known "even/odd" isotopic effects specific to FAs, variations in RQCs (according to their position in the chain, interspectral comparison of the various UFAs (mono- or polyunsaturated) (see **Figure 17**). Given the absence of significant chemical dispersion, assignment of $CH_2$ groups for SFAs is much more difficult. To achieve this, two additional approaches can be combined and applied: i) the reductive and regioselective dideuteration of the **ML** from methyl petroselenate (at positions 6 and 7) and **MO** (at positions 9 and 10); ii) the theoretical prediction of $^2$H-RQCs along the chain by computer modelling. The first one provides key information on the magnitude of RQCs in the middle of the sidechain, the second one (detailed below) made possible to model the orientational behaviour of the chain in an achiral mesophase (PBG), and compared the predicted RQCs values with experimental ones (see **Figure 16b**) [**73**].

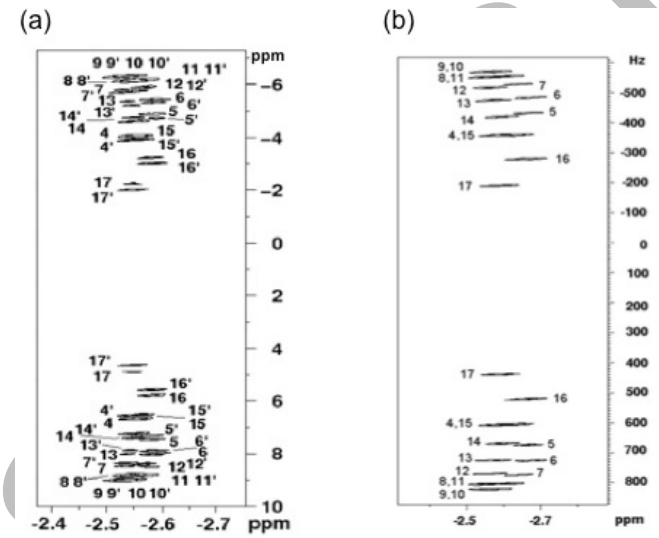


**Figure 16.** Expansion on the tilted 2D map of the methylenic of **MS** in (a) PBLG/Py and (b) PBG/Py. Values (in ppm) of $F_2$ axis have no spectral meaning. Figure adapted from ref. **73** with permission.

### *10.2 Computer modelling of orientational ordering of SFAs*

The computational approach developed combines both a conformational sampling of the solute and the $^2$H-RQC prediction (in an achiral environment) based on a model dominated by steric repulsion between the FA and the $\alpha$-helical polypeptide. Here the PBLG fibres are modelled as an infinitely long cylinder solid [**73**]. The model makes it possible to adequately reproduce the experimental $^2$H-RQC value, providing an effective tool to assign the QDs, but also to understand the phenomena orientation of SFAs in a polypeptide mesophase oriented in the magnetic field.

POSTPRINT

In the proposed model (derived from model developed for the prediction of RDCs), the expression for the $S_{C\text{-}D_i}$ local order parameter (for a given conformer $\mathcal{J}$) is obtained using **Eq. 6** [**73,74,75**],

$$S^{J}_{C-D_i} \approx -\frac{3}{8\pi} S_p \int \cos^2\theta_{C-D_i}(\omega') \frac{\delta a_{excl}}{a_p} d\omega' - \frac{1}{2} \qquad (6)$$

where the integral is over all possible solute orientations ($\omega'$) with respect to the rod mimicking the polypeptide helix. In **Eq. 6**, $S_p$ is the order parameter of the polypeptide, which is close to one [**76**], while $a_p$ is the area *per* polymer in the solution and $\delta a_{excl}$ is the area excluded to the centre of mass of the solute by the polypeptide. Computational calculations can be limited to a plane since, if a polypeptide is represented as an infinite rod, the excluded volume is independent of the solute position along its axis. The final value of the integral depends on the shape of the solute and vanishes for spherical compounds. As a consequence, non-zero values of $S_{C\text{-}D_i}$ can be only obtained for anisometric solutes.

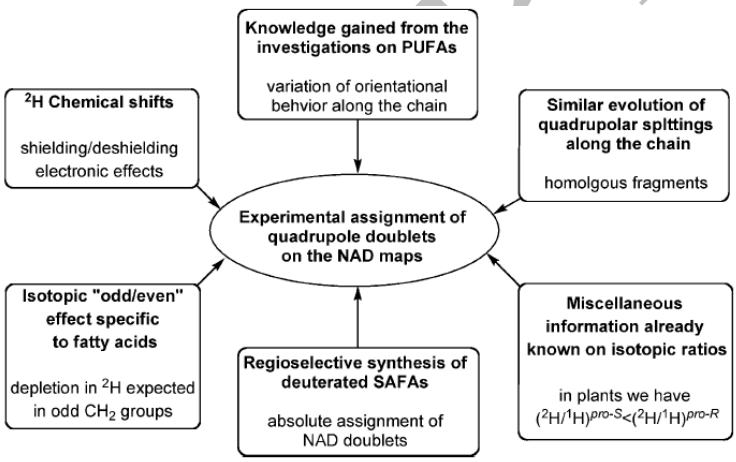


**Figure 17**. Multi-factor strategy for experimentally assigning the QDs on ANAD 2D spectra. Figure reproduced from ref. **73** with permission.

FAMEs are highly flexible molecules, and therefore they cannot be identified by a single geometry. For such molecules, Rotational Isomeric State (RIS) approximation can be adopted, assuming that a flexible solute can be treated in terms of its stable conformational states (conformers) [**77**]. Thus the $S_{C\text{-}D_i}$ order parameters are evaluated over all the considered conformers with **Eq. 7**,

$$S_{C-D_i} = \sum_J w_J S^J_{C-D_i}, \qquad (7)$$

where $S^J_{C-D}$ is the order parameter calculated for the $\mathcal{J}^{th}$ conformer, calculated according to **Eq. 4**, and $w_{\mathcal{J}}$ is the statistical weight of this conformer. Since the conformational distribution is expected to be

negligibly affected by the weakly aligning environment [**78**]; this weight can be simply evaluated on the basis of the torsional potentials, $V_J$.

$$w_J = \frac{\exp(-V_J / k_B T)}{\sum_M \exp(-V_M / k_B T)} \qquad (\mathbf{8})$$

where $T$ is the absolute temperature and $k_B$ is the Boltzmann constant.

In practice, the computational procedure encompasses three steps: (i) Monte Carlo (MC) sampling (50 000 steps) of the RIS conformers of FAMEs (obtained by DFT calculation with the B3LYP functional and the 6-31G** basis set) in agreement with the Metropolis algorithm [**79**]; (ii) calculation of $S^J_{C-D}$ order parameters for all the C-D bonds of each retained conformer; (iii) evaluation of averaged $S_{C-D}$ values by **Eq. 5**, and finally the $^2$H-RQCs according to **Eq. 2**.

The predicted $S_{C-D}$ and hence the RQC values were found to be negative, confirming the positive sign of the ($^{13}$C-$^1$H)-RDCs along the chain determined experimentally (measured on the proton-coupled $^{13}$C 1D spectra in PBG/Py). Both results indicated that C-D bonds have a preference to lie perpendicular, rather than parallel to the director of the phase, which also coincides with the average polypeptide axis.

Finally, the predicted variation profiles (a sine bell pattern) of RQCs for the three SFAs were similar, and nearly symmetric with respect to the centre of the chain. This particular trend of $S_{CD}$ reflects the

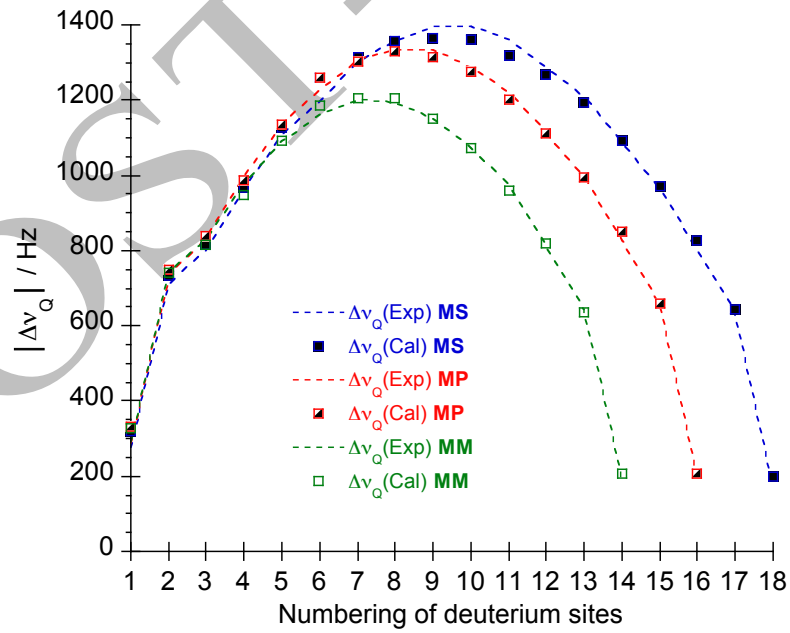


**Figure 18.** Experimental (dashed lines) and predicted (symbols) absolute values of $\Delta\nu_Q$'s as a function of the chain position, for **MM**, **MP** and **MS** oriented in PBG/Py at 300 K. Figure reproduced from ref. **73** with permission.

POST-PRINT

gradient of internal freedom on moving from the ends to the centre of lipid chains. Thus, the C-D bonds close to chain terminals, having higher motional freedom than those located in the central part of the chain, are less oriented. Such a bell-shaped profile, along with an increase of order parameters with the chain length, had been predicted by the random flight chain model of linear homopolymers in the presence of steric obstruction [**80,81**].

As deduced from plots of **Figure 18**, an excellent agreement between the experimental and the predicted computational values of QD for the three SFAs have been obtained, allowing a clear final assignment of QDs detected on the 2D map in PBG (see **Figure 16b**), that in turn was used to assign the pairs of QDs in the 2D map in PBLG (see **Figure 16a**).

Finally, the comparison of the variations of RQCs *versus* $^2$H site in SFAs and UFAs (see **Figures 9** and **18**) shows that no discontinuity in ordering of SFAs is observed, thus confirming the effect of the rigid linker(s) at the middle of chain in UFAs and the orientational decorrelation of the two fragments.

## 11. Homogeneous triglycerides: the last frontier?

The analytical potential of ANAD 2D-NMR was successively tested for studying on molecules of increasing complexity (BPTH, (P/C)UFAs and then SFAs). As a last frontier to be crossed, the case the homogeneous triglycerides (TGs), the last class of lipids, has been explored.

Given their structure, the analysis of anisotropic ANAD spectra of homogeneous TGs (three identical lipid chains) is *a priori* much more complex than that of the corresponding isolated FAs [**82**]. However, if the overlapping rate of the lines remains "reasonable", the determination of the isotopic profile along the alkyl chain could be considered without the step of transesterification of TG to glycerol and FAME being necessary. Two homogeneous saturated TGs, i.e. containing three identical saturated alkyl chains, were tested: the tributyrin (**TB**, C-4) (see **Figure 19a**) and the trimyristin (**TM**, C-14) [**82**].

In accordance with Altmann's definition [**61**], homogeneous, TG are flexible molecules of $C_s$ symmetry on average containing a plane of symmetry σ. They have two enantiotopic side chains whose hydrogenated sites are diastereotopic and a central chain (that is diastereotopic relative to the two side chains) whose hydrogenated sites are enantiotopic. All the stereochemical relationships of **TB** are illustrated in **Figure 19a**. Such a situation disappears, of course, in the case of heterogeneous TG where the three chains are different.

As shown in **Figure 19b**, only seven resonances corresponding to the diastereotopic sites of **TB** were observed in achiral isotropic NMR, representing only 50% of the molecule's unequivalent deuterium sites. The interest of chiral ANAD NMR was therefore to be able to discriminate between the two lateral enantiotopic, a and c, as well as the enantiotopic C-H directions in the central chain b. The large

POST-PRINT

number of QDs expected on the NAD spectra of **TG** if all (possible) $^2$H sites are spectrally differentiated (*i.e.* 20 and 80 QDs for **TB** and **TM**) implies that they cannot be analysed without the help of QUOSY 2D experiments.

The analysis of the series of 1D-NMR extracted subspectra from the *Q*-COSY Fz NAD map of **TB** recorded in PBLG/Py indicates that 95% of the unequivalent $^2$H sites (*i.e.* 19 QDs out of 20) are spectrally discriminated (see **Figure 20**).

Due the conformational dynamics of chains, only the terminal enantiotopic methyl pair (4a/4c) is not really discriminated, although an asymmetric deformation of the two components of QD certainly indicates a slight difference in $^2$H-RQC values. While comparison with **TB** spectra recorded in the achiral mesophase (PBG/Py) allows the QD pairs corresponding to the enantiotopic pairs to be assigned, the AC determination of signal remains arbitrary. In this example, the number of differentiated sites are in agreement with the theoretical number expected for a $C_s$-symmetry molecule, which implies that the shape recognition phenomena involved in the polypeptide discrimination mechanisms differentiate the central chain from the two side chains (see **Figures 19a/b**) [**82**]. For **TM**, the situation was much less favourable since only about twenty QDs out of the theoretically expected 80 were observed (no signal detected for the glyceryl fragment sites). Deeper analysis of the results has indicated that the molecule behaves like a $C_{3v}$-symmetry molecule and no longer has a $C_s$-symmetry on average. In other words, the enantiorecognition mechanisms no longer distinguish the side chains (a and c) from the central chain (b) (see **Figure 19a/d**). This situation occurs when the ratio ($V_{a,c}/V_b$) of the persistent molecular volume of the side chain ($V_{a,c}$) to the central chain ($V_b$) where V is the 3D space explored by the moving atoms of chains), tends strongly towards unity. Obviously, this ratio tends rapidly towards one, when the number of methylene groups becomes large, while only one $CH_2$ group differentiates the two types of chain (case of **TM**) [**82**]. Under this condition, the global shape of the TG formally tends toward a $C_{3v}$-symmetry (instead of a $C_s$-symmetry), leading to the absence of differentiation of three chains. These changes of effective orientational behaviour point out the importance of the size and shape difference between lateral and central alkyl chains of the TGs, towards the shape recognition mechanisms involved in the enantiodiscrimination phenomena. Whatever the helically chiral polymer used, the sensitivity of shape recognition mechanisms is one of key parameters governing the efficiency of enantiodifferentiation [**28, 81**].

POST-PRINT

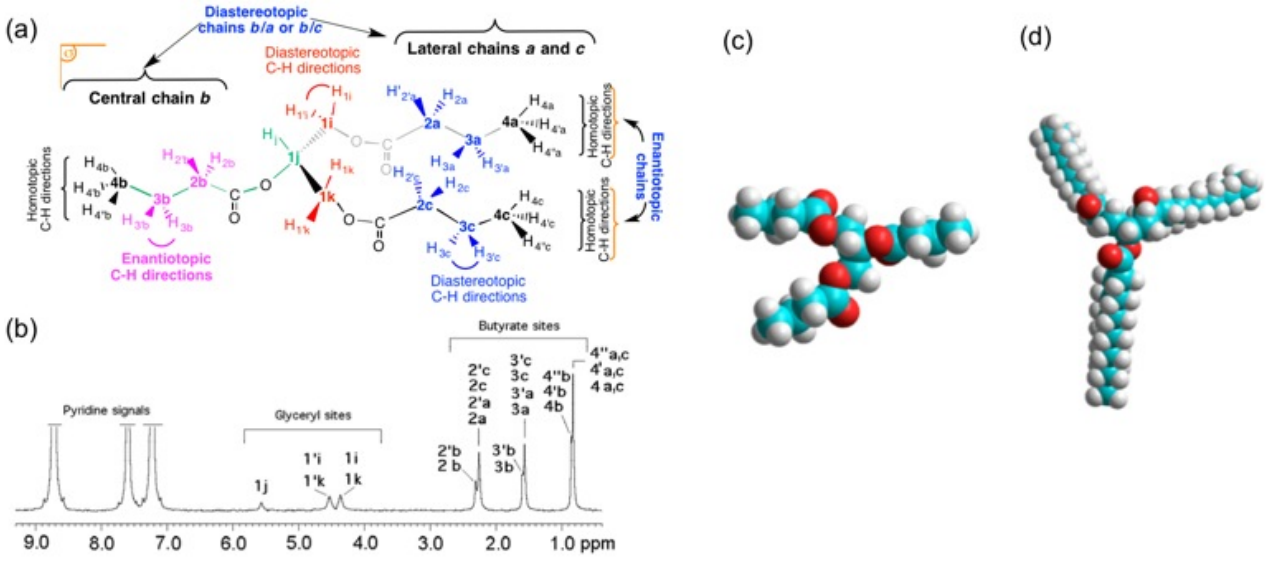


**Figure 19.** (a) Atomic numbering and stereochemical relationships between the different hydrogenated sites of the glyceryl part (sites i, j, k) and methylene (2 and 3) and methyl (4) groups of the three hydrocarbon chains (a, b and c) of **TB**. (b) NAD 1D-NMR spectrum (92.1 MHz) recorded in 310 K in pyridine. (c and d) Computational 3D structures of the *« all-trans »* conformer of **TB** and **TM**, performed using the semi-empirical method PM3 available in Hyperchem software (release 8.0.6). Figures adapted from ref. **82** with permission.

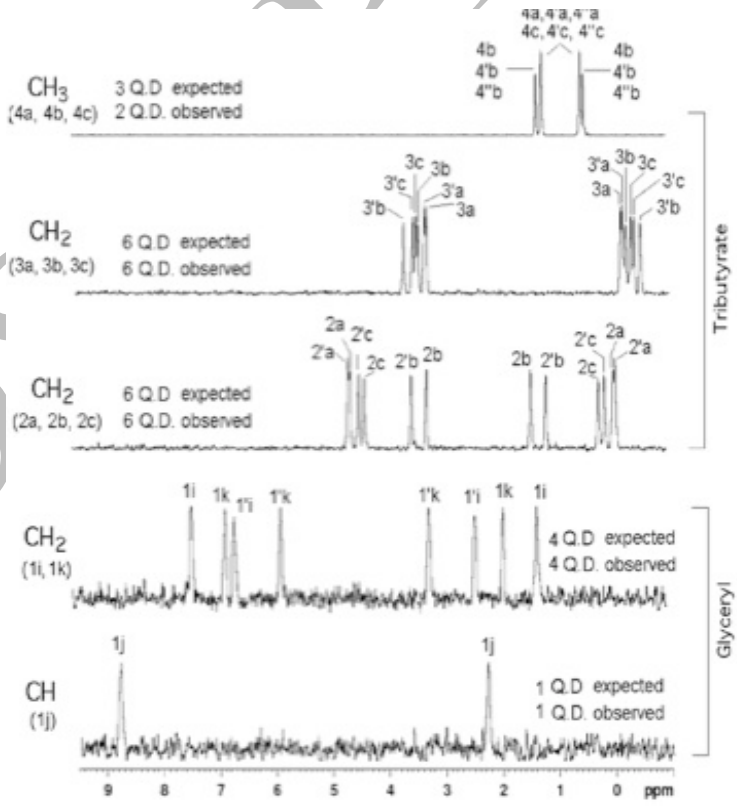


**Figure 20.** Series of 1D NAD subspectra extracted from the tilted *Q*-COSY Fz map (92.1 MHz) of **TB** recorded in PBLG/Py. at 300 K. The assignment of QDs in relation to the various diastero- and enantiotopic positions is arbitrary. Figure adapted from ref. **81** with permission.

## 12. Biochemical investigations

### *12.1 The FAS and desaturases*

The analytical interest of anisotropic $^2$H 2D-NMR for isotopic monitoring has proved extremely useful in studying and understanding the origin of hydrogen atoms at enantiotopic sites during the biosynthesis of saturated (**MS**) and unsaturated fatty acids (**ML**) in the case of *Fusarium lateritium*, an oil-bearing fungus [**81**]. In practice, the **ML** was isolated from *Fusarium lateritium* grown in a medium not enriched in deuterium (reference medium) and then in the presence of water and various substrates slightly enriched (selectively) in deuterium: glucose[6,6-$^2H_2$], glucose[1-$^2$H] and sodium acetate[2-$^2H_3$] in order to compare the two sets of results and to deduce the $^2$H incorporation pathway.

The distribution pattern of $^2$H in a product can be obtained by quantitative $^2$H NMR (isotropic or anisotropic) of this analyte in natural abundance or slightly enriched in $^2$H, typically 2 to 5 times the value of natural abundance to avoid significant KIEs. The links between the ratios $(^2H/^1H)_i$ measured in the product and the different possible hydrogen sources can be quantified using a simple linear model. This describes the amount of hydrogen transferred to each position from each position of the substrate or water in the medium. Thus, the site-specific isotopic ratio at position i, $(^2H/^1H)_i$, of a product can be defined by the relationship [**83**],

$$\left(\frac{^2H}{^1H}\right)_i^{prod} = a_{im}\left(\frac{^2H}{^1H}\right)_m + \sum_j a_{ij}\left(\frac{^2H}{^1H}\right)_j^{subs}, \qquad (\mathbf{9})$$

where $(^2H/^1H)_m$ and $(^2H/^1H)_j$ are respectively the isotopic ratios of the medium (water) and at a given site j of the substrate. The isotopic redistribution coefficients, $a_{im}$ (product medium) and $a_{ij}$ (product substrate) provide a quantitative description of the various relationships reflecting both the amount of hydrogen (deuterium) transferred from a given site and the KIEs for a set of biochemical reactions [**81**]. The resolution of the different equations makes it possible to interpret the origin of the hydrogen atoms.

The isotopic ratios $(^2H/^1H)$ for each pro-*R* and pro-*S* position of the different even and odd methylene groups in the **ML** chain thus made it possible to calculate the isotopic redistribution coefficients $(a_{ij})$ that characterize the specific sources of hydrogen atoms (not exchangeable) of glucose but also of water in the medium. In addition, the stereoselectivity of the mechanisms involved during the introduction or extraction of hydrogen atoms along the FA chain has been determined for the first time. Four important characteristics associated with the enzymatic mechanisms leading to **ML** have been demonstrated. These results can be summarised as follows: i) for the even positions of the methylenes, the hydrogen atoms (deuterium) of stereochemistry s (pro-*S* site) come only from water (by protonation), while those of (*R*)-

POST-PRINT

stereochemistry (pro-*R* site) come (mainly) from water molecules due to the "post-malonate" exchange but also to a lesser extent from sodium acetate; ii) the non-glucose exchangeable hydrogen atoms (at least at positions 6,6 and 1) are transferred to the $CH_2$ in odd position via the NAD(P)H/$H^+$ pool, *i.e.* the co-factors used by the two reductases involved in the elongation steps of the AG chain; iii) all hydrogen atoms removed at sites 9/10 and 12/13 during the desaturation steps via desaturases $\Delta^9$ and $\Delta^{12}$ are of (*R*)-stereochemistry (pro-*R* hydrogenated site); iv) during these two desaturations, a secondary KIE occurs [**83,84**].

### *12.2 Comparison of two $\Delta^{12}$-epoxydases*

In a second case study, NAD 2D-NMR in CLCs was applied to highlight possible mechanistic differences in the biosynthesis of vernoleic acid from linoleic acid (in two plant families: the Euphorbiaceae (*Euphorbia lagascae*) and the Asteraceae (*Crepis palaestina, V. galamensis*) [**85**]. The intriguing question here, was how these diverse reactions and reaction centres might affect $(^2H/^1H)_i$ isotopic ratios in the substrates and products involved.

In this second application work, the relative variations in the natural site-specific isotopic fractionation $(^2H/^1H)_i$ have was used to determine whether distinct characteristics at the reaction centre could be revealed by comparing and analysing the differences in the isotopic profile of the substrate, the **ML**, and the epoxidation product, the **MV** [**85**]. Although *E. lagascae* and *V. galamensis* use different enzymes to achieve epoxidation of the **ML** in position 12 (a cytochrome P450 monooxygenase in the first case [**86**], and a di-iron dioxygenase in the second [**87**]), it has been demonstrated that the **ML** and **MV** isolated from the seeds of the two plants have remarkably similar isotopic profiles (see **Figure 21**) [**85**]. This

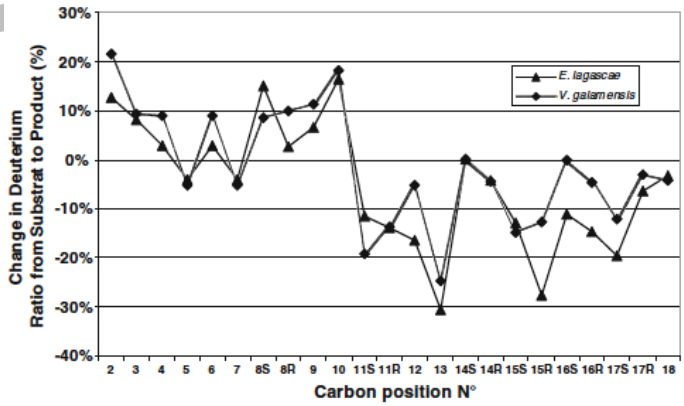


**Figure 21.** Variations in isotope ratios (in percent) between substrate (**ML**) and product (**MV**) observed when these UFAs are extracted from *V. galamensis* and *E. lagascae*. Note the enrichment and then the overall deuterium depletion on the $C_2$-$C_{10}$ fragment and $C_{11}$-$C_{17}$ one, respectively. Figure reproduced from ref. **85** with permission.

POST-PRINT

similarity has been interpreted as indicating that the dominant feature of the reaction mechanism is the involvement of activated Fe, while the architecture of the active site seems to play a much less important role as expected [**85**].

## 13. Conclusions and prospects

NAD 2D-NMR in ALCs and CLCs is a unique and original tool for accessing isotopic information that is inaccessible by the traditional SNIF-NMR™ method. The series of results opened wide prospects in the domain of the isotope fractionation analysis by NAD NMR. In particular, the determination of the enantio-isotopomeric excesses (*eie*'s) along the entire flexible chain, and the assignment of the major enantio-isotopomer for **ML** is a valuable achievement and this finding paves the way for new various applications. For the first time, it is now possible to model the enzymatic mechanisms leading to the different FAs classes by incorporating the enantioselective properties of the enzymes involved.

In the case of FAs, homopolypeptides CLCs prepared with polar co-solvents (Py or DMF) allowed to optimize the dispersion of QD on 2D maps and/or to maximize the number of enantiotopic sites discriminated against by the molecule. However, with the exception of **ML**, there is no single chiral mesophase capable of discriminating all inequivalent $^{2}H$ signals for the different classes of AG or TG. One challenge of the FA project was to find a chiral mesophase that could produce NAD spectra where all inequivalent $^{2}H$ sites are optimally discriminated for all types of FAMEs. This aim was partly succeeded in the sense that we have significantly increased the percentage of discriminated $^{2}H$ sites compared to our previous investigations. However, the various results obtained illustrated the versatility and the subtle balance between orientational phenomena and enantio-differentiation mechanisms for flexible, long prochiral chains that are characterised by complex internal conformation dynamics.

Beyond the project on the FAs, two innovative applications of ANAD NMR to the isotopic analysis of molecules of interest have recently been described, one associated with the analysis of a geological biomarker (miliacin) involved in studying the evolution of climatic conditions [**88**], the second concerning the fight against counterfeiting (vanillin) [**24**].

There is no doubt that the future will require a further increase in the sensitivity of ANAD's NMR. Indeed, as any NMR investigations involving weakly abundant/low sensitive nuclei, the need of enhanced-sensitivity experiments is crucial for exploring the frontiers of ANAD NMR. ANAD experiments by using very high-field NMR spectrometers ($B_o$ > 14 T) and still equipped by a $^{2}H$ cryoprobe is the most direct way to overcome the sensitivity problem, rendering the accuracy of isotopic ratio measurements higher. For a much lower financial cost, the recording of anisotropic ANAD 2D spectra using new $^{2}H$ signals-acquisition protocols such as non-uniform sampling (NUS) [**89,80**]

POST-PRINT

combined with special data reconstruction processing (Cov or CST) method instead of conventional Fourier transformation) is a possible approach to develop and to apply in the nearest future [**91,92**].

## 14. Special acknowledgments and contextual comments

The work associated to the project "Fatty acids" presented in this review involves both international, national and internal scientific collaborations, including Dr. Alberta Ferrarini from the University of Pisa (Italy), Drs. Isabelle Billault, Drs. Steven Le Feunteun and Richard Robins from the CEISAM laboratory at the University of Nantes (France) but also Dr. Christie Aroulanda (ICMMO), and the various contributions of Ph.D students became now Doctors in Science: Dr. Andrea Borgogno (Italy), Drs. Christie Aroulanda and Zeinab Serhan (France) and Dr. Vincent Baillif (France) or Master students Emmanuel Chefdeville, Alicia Le Du, Laura Martel, Minale Ouethrani (France).

This long-term interlaboratory project involved various expertise domains (NMR spectroscopy, computational modelling, chemistry, biochemistry) and lead to nine research articles published in various scientific journals to date. It was made possible thanks to the recurrent funding of the basic research by the CNRS, but also by the universities of Paris-Sud, Nantes and Pisa; the two attempts at funding by national agencies (such as ANR in France) having failed.

Indirectly, this work was also possible with the help of the Bruker NMR compagny (at "the end of the last century") for the specific manufacturing and the loan of a 5-mm, Selective EXcitation $^{2}H$ probe ("SEX" probe), essential to explore and collect the first successes of NAD NMR at 9.4 T (in particular on BPTH), thus leading a few years later to the financing of a 14-T NMR spectrometer equipped to a 5-mm, selective cryogenic $^{2}H$ probe.

Thank you also to Prof A. Loewenstein of Technion (Haifa, Israel) who transferred his knowledge of polypeptide liquid crystals in the 1990s. I am grateful to Prof. Jacques Courtieu (University of Paris-Sud)) and Prof. James W. Emsley (University of Southampton, UK) who both initiated me to the fantastic world of NMR spectroscopy in liquids crystals during my Thesis and post-doctoral research. Thanks to Dr. Jean-pierre Bayle for the critical reading of the manuscript.

## 15. Dedication

Associated to this publication, I would like to personally dedicate this review to Prof. Zeev Luz (see **Figure 22**) of the Weizmann Institute (Rehovot) for his continous and impressive contribution to NMR spectroscopy and the development of NMR in CLs over the past four decades [**9**]. It was an honour and a real "mind pleasure" to collaborate with him (in Orsay and Rehovot) wihtout forgotting his "favourite chemist", Herbert Zimmermann of Max Planck Institute of Heidelberg, the "emperor" of the selective

POST-PRINT

deuteration, during almost 15 years on several projects. Almost all of them were related to the enantiodiscrimination phenomenon in lyotropic CLCs [**41**]. No spectroscopists "playing" or with anisotropic NMR should ignore what Zeev Luz has brought in the domain!


**Figure 22.** Zeev Luz working at his office. On the right side of the image, his special optical apparatus having a lens for zooming on written documents [**9**]. Picture taken during my stay at the Weizmann Institute in 2007. Photo credit: Philippe Lesot.

POST-PRINT

## 15. References

[**1**] Remaud G. Recent development of NMR for isotope profiling. Eur. Pharm. Rev. 2014;**9**: 46-49.

[**2**] Martin G, Martin M-Y. Deuterium labelling at natural abundance level as studied by high field quantiative $^{2}$H NMR. Tetrahedron Lett. 1981;**22**:3525-3528.

[**3**] Martin G, Zhang B-L, Naulet N, Martin M. Deuterium transfer in the bioconversion of glucose to ethanol studied by specific isotope labeling at the natural abundance level. J Am Chem Soc. 1986;**108**:5116-5122.

[**4**] Martin GG, Wood R, Martin GJ. Detection of added beet sugar in concentrated and single strength fruit juices by deuterium nuclear magnetic resonance (SNIF-NMR) method: collaborative study. J AOAC Int. 1996;**79**:917-28.

[**5**] Jamin E, Thomas F. SNIF-NMR Applications in an economic context: fraud detection in food products, in: G.A. Webb (Ed.) Modern Magnetic Resonance, Springer International Publishing, 2017, pp. 1-12.

[**6**] Remaud GS, Martin Y-L, Martin GG, Martin GJ. Detection of sophisticated adulterations of natural vanilla flavors and extracts: Application of the SNIF-NMR method to vanillin and *p*-hydroxybenzaldehyde. J Agric Food Chem. 1997;**45**:859-866.

[**7**] Fronza G, Fuganti C. Natural abundance $^{2}$H nuclear magnetic resonance study of the origin of raspberry ketone. J Agric Food Chem. 1998;**46**:248-254.

[**8**] Jézéquel T, Valentin Joubert, V, Giraudeau P, Remaud GS, Akoka S. The new face of isotopic NMR at natural abundance. Magn Reson Chem. 2017;**55**:77-90.

[**9**] Samulski E. Zeev Luz (1932–2018). Liquid Crystals. 2019; online: DOI: 10.1080/02678292.2019.1555930.

[**10**] de Laeter JR, Böhlke JK, De Bièvre PH, Hidaka H, Peiser HS, Rosman KJR, Taylor P. Atomic weights of the elements: Review 2000 (IUPAC Technical Report). Pure & Appl Chem. 2000;**75**:683–799.

[**11**] Cordela C, Moussa I, Martel AC, Sbirrazzuoli N, Lizzani-Cuvelier L. Recent developments in food characterization and adulteration detection: technique-oriented perspectives. J Agric Food Chem. 2002;**50**:1751-64.

[**12**] Zhang BL, Pionnier S. A simple method for the precise and simultaneous determination of primary and multiple secondary kinetic deuterium isotope effects in organic reactions at natural abundance. J Phys Org Chem. 2001;**14**:239-246.

[**13**] Zhang BL, Yunianta, Martin ML. Site-specific isotope fractionation in the characterization of biochemical mechanisms. The glycolytic pathway. J Biol Chem. 1995;**270**:16023-16029.

[**14**] Zhang BL, Stephan Buddrus, Martin ML. Site-specific hydrogen isotope fractionation in the biosynthesis of glycerol. Bioorg Chem. 2000;**28**:1-15.

[**15**] Pionnier S, Robins R, Zhang BL. Natural abundance hydrogen isotope affiliation between the reactants and the products in glucose fermentation with yeast. J Agr Food Chem. 2003;**51**:2076-2082.

[**16**] Zhou YP, Zhang BL, Stuart-Williams H, Grice K, Hocart CH, Gessler A, Kayler ZE, Farquhar GD. On the contributions of photorespiration and compartmentation to the contrasting intramolecular $^{2}H$ profiles of C3 and C4 plant sugars. Phytochemistry 2018;**145**:197-206.

[**17**] Legrand F, Rémaud G, Akoka S. Natural abundance $^{2}H$-ERECTIC NMR authentication of the origin of methyl salicylate. J Agric Food Chem. 2005;**53**:5125-5129.

[**18**] Martin ML, Martin GJ, Deuterium NMR in the study of site-specific natural isotope fractionation. (SNIF-NMR) in NMR basic principles and progress Diehl P, Fluck E, Gunther H, Kosfeld R, Seeling J. Editors. Springer Verlag, Berlin,1991;**23**:1-61.

[**19**] Hagedorn ML, Differentiation of natural and synthetic benzaldehydes by $^{2}H$ nuclear magnetic resonance. J Agric Food Chem. 1992;**40**:634-637.

[**20**] Remaud GS, Martin Y-L, Martin GG, Naulet N, Martin GJ. Authentication of mustard oils by combined stable isotope analysis (SNIF-NMR and IRMS). J Agric Food Chem. 1997;**45**:1844-1848.

[**21**] Gonzalez J, Jamin E, Martin Y-L, Martin GG, Martin ML. Authentication of lemon juices and concentrates by a combined multi-isotope approach using SNIF-NMR and IRMS. J Agric Food Chem 1998;**46**:2200-2205.

[**22**] Tenailleau E, Lancelin P, Robins RJ, Akoka S. Authentication of the origin of vanillin using quantitative natural abundance $^{13}C$ NMR. J Agric. Food Chem. 2004;**52**:7782-7787.

[**23**] Remaud GS, Akoka S. A review of flavors authentication by position specific isotope analysis by nuclear magnetic resonance spectrometry: the example of vanillin. Flav Frag J. 2016;**32**:77-84.

[**24**] Texier-Bonniot T, Berdagué P, Robins R, Remaud G, Lesot P. Analytical contribution of deuterium 2D-NMR in oriented solvents to $^{2}H/^{1}H$ isotopic characterization: the case of vanillin. Flav Frag J. 2018;**34**:217-229.

[**25**] Billault I, Guiet S, Mabon F, Robins RJ. Natural deuterium distribution in long-chain fatty acids is nonstatistical: a site-specific study by quantitative $^{2}H$ NMR spectroscopy. ChemBioChem. 2001;**2**:425-431.

[**26**] Lesot P, Aroulanda C, Billault I. Exploring the analytical potential of NMR spectroscopy in chiral anisotropic media for the study of the natural abundance deuterium distribution in organic molecules. Anal Chem. 2004;**76**:2827-2835.

[**27**] Emsley JW, Lindon JC in NMR spectroscopy using liquid crystal solvents, Pergamon press, Oxford, 1975.

[**28**] Sarfati M, Lesot P, Merlet D, Courtieu J. Theoretical and experimental aspects of enantiomeric differentiation using natural abundance multinuclear NMR spectroscopy in polypeptide liquid crystals. Chem. Commun. 2000;2069-2081.

[**29**] Lesot P, Sarfati M, Courtieu J. Natural abundance deuterium NMR spectroscopy in polypeptide liquid crystals as a new and incisive means for enantiodifferentiation of chiral hydrocarbons. Chem Eur J. 2003;**9**:1724-1745.

POST-PRINT

[**30**] Lesot P. Courtieu J. Natural abundance deuterium NMR spectroscopy: developments and analytical applications in liquids, liquid crystals and solid phases. Prog Nucl Magn Reson Spectrosc. 2009;**55**:128-159.

[**31**] Lesot P, Deuterium NMR of Liquid-crystalline samples at natural abundance, Encyclopedia of Magnetic Resonance (eMagRes), 2013;**2**:315-334, J Wiley: Chichester, Ed. Harris RK.

[**32**] Lesot P, Berdagué P, Meddour A, Kreiter A, Noll M, Reggelin M, $^{2}H$ and $^{13}C$ NMR-based enantiodetection using polyacetylene *versus* polypeptide aligning media: versatile and complementary tools for chemists. ChemPlusChem, 2019; online: DOI: 10.1002/cplu.201800493.

[**33**] Briggs JM, Farnell LF, Randall EW. Proton-noise-decoupled deuterium resonance at natural abundance by Fourier-transform. Chem Commun. 1973;70-71.

[**34**] Khetrapal CL, Ramanathan KV, Suryaprakash N. Vivekanandan S, Natural abundance $^{2}H$ NMR spectra of molecules oriented in liquid crystals. J Magn Reson. 1998;**135**:265-266.

[**35**] Lesot P, Merlet D, Loewenstein A, Courtieu J. Enantiomeric visualisation using proton-decoupled natural abundance deuterium NMR in poly-γ-benzyl-L-glutamate liquid crystalline solutions. Tetrahedron: Asym. 1998;**9**:1871-1881.

[**36**] Kovacs H, Moskau D, Spraul M. Cryogenically cooled probes, a leap in NMR technology. Prog Nucl Magn Reson Spectrosc. 2005;**45**:131-155.

[**37**] Eliel EE, Wilen SH, in Stereochemistry of Organic Compounds, J. Wiley & Sons, INC, New York, 1994.

[**38**] Rothchild R, NMR methods for determination of enantiomeric excess. Enantiomer, 2000;**5**:457-471.

[**39**] Wenzel J, in Discrimination of Chiral Compounds using NMR Spectroscopy. J. Wiley & Sons, 2007.

[**40**] Wenzel TJ, Chisholm CD. Using NMR spectroscopic methods to determine enantiomeric purity and assign absolute stereochemistry. Prog Nucl Magn Reson Spectrosc. 2011;**59**:1-63.

[**41**] Lesot P, Aroulanda C, Zimmermann H, Luz Z. Enantiotopic discrimination in the NMR spectrum of prochiral solutes in chiral liquid crystals. Chem. Soc. Rev. 2015;**44**:230-275.

[**42**] Meddour A, Canet I, Loewenstein A, Péchiné J-M, Courtieu J. Observation of enantiomers, chiral by virtue of isotopic substitution, through deuterium NMR in a polypeptide liquid crystal. J Am Chem Soc. 1994;**116**:9652-9656.

[**43**] Aroulanda A, Merlet D, Courtieu J, Lesot P. NMR experimental evidence of the differentiation of enantiotopic directions in $C_s$ and $C_{2v}$ molecules using partially oriented, chiral media. J Am Chem Soc, 2004;**123**:12059-12066.

[**44**] Merlet D, Emsley JW, Lesot P, Courtieu J. The relationship between molecular symmetry and second-rank orientational order parameters for molecules in chiral liquid crystalline solvents. J Chem Phys. 1999;**111**:6890-6896.

[**45**] Lafon O, Lesot P, Zimmermann H, Poupko R, Luz Z. Chiral discrimination in the $^{13}C$- and $^{2}H$-NMR of the crown and saddle isomers of nonamethoxy-cyclotriveratrylene in chiral liquid-crystalline solutions. J Phys Chem B. 2007;**111**:9453-9467.

[**46**] Lesot P. Aroulanda C, Luz Z. Analysis of the enantiotopic discrimination in the NMR spectra of prochiral solutes dissolved in chiral liquid crystals by symmetry factorization of the saupe ordering matrix. J Chem Phys. 2009;**131**:104501/1-16.

[**47**] Merlet D, Ancian B, Courtieu J, Lesot P. Two-dimensional deuterium NMR spectroscopy of chiral molecules oriented in a polypeptide liquid crystal: application for the enantiomeric analysis through natural abundance deuterium NMR, J Am Chem Soc. 1999;**121**:5249-5258.

[**48**] Lafon O, Lesot P, Merlet D, Courtieu J. Modified z-gradient filtering as a new mean to obtain phased deuterium autocorrelation 2D-NMR spectra in oriented solvents. J Magn Reson. 2004;**171**:135-142.

POST-PRINT

[**49**] Lesot P, Lafon O. Enantiomeric Analysis using natural abundance deuterium 3D-NMR spectroscopy in polypeptide chiral oriented media. Chem Phys Lett. 2004;**458**:219-222.
[**50**] Lesot P, Lafon O, Experimental detection of achiral and chiral naturally abundant $^{13}C$-$^{2}H$ isotopomers by 2D-NMR in liquids and chiral oriented solvents. Anal Chem. 2004;**84**:4569-4573.
[**51**] Aroulanda C, Sarfati M, Courtieu J, Lesot P. investigation of enantioselectivity of three polypeptide liquid-crystalline solvents using NMR spectroscopy. Enantiomer, 2001;**6**:281-287.
[**52**] Lesot P, Lafon O, Aroulanda C, Dong R. $^{2}H$ NMR studies of two-homopolypeptide lyotropic mesophases: toward the quantification of solute-fiber interactions. Chem Eur J. 2008;**14**:4082-4092.
[**53**] Masarwa A, Gerbig D, Oskar L, Loewenstein A, Reisenauer HP, Lesot P, Schreiner PR, Marek I. Probing the limits of NMR and VCD spectroscopy in the stereochemical assignment of chiral $^{2}H_{6}$-neopentane. Angew Chem Int Ed. 2015;**54**:13106-13109.
[**54**] Arnold L, Marx A, Thiele C-M. Reggelin M. Polyguanidines as chiral orienting media for organic compounds. Chem Eur J. 2010;**16**:10342-10346.
[**55**] Li GW, Cao JM, Zong W, Hu L, Hu ML, Lei X, Sun H, Tan RX. helical polyisocyanopeptides as lyotropic liquid crystals for measuring residual dipolar couplings. Chem Eur J. 2017;**23**:7653-7656.
[**56**] Reller M, Wesp S, Koos M R M, Reggelin M, Luy B. Biphasic Liquid Crystal and the Simultaneous Measurement of Isotropic and Anisotropic Parameters by Spatially Resolved NMR Spectroscopy, Chem Eur J. 2017;**23**:13351-13359.
[**57**] Meyer N-C, Krupp A, Schmidts V, Thiele C-M, Reggelin M. Polyacetylenes as enantiodifferentiating alignment media. Angew Chem Int Ed. 2012;**51**: 8334-8338.
[**58**] Burr GO, Burr MM, Miller E. On the nature and role of the fatty acids essential in nutrition. J Biol Chem. 1930;**86**:587-621.
[**59**] Stryer L. in Biochemistry (4th Ed.), Chap. "Fatty acid metabolism", New York: Freeman W.H. and Company. (1995).
[**60**] Moss GP, Smith PAS, Tavernier D. IUPAC Compendium of chemical terminology. pure and applied chemistry (2nd ed.). International Union of Pure & Applied Chemistry. 1997;**67**:1307-1375.
[**61**] Altmann, SI. The summary of nonrigid molecules: the Schrödinger supergroup. Proc Roy Soc. (London). 1967;**A298**:184-203.
[**62**] Lesot P, Baillif V, Billault I. Combined analysis of four C-18 unsaturated fatty acids using natural abundance deuterium 2D-NMR spectroscopy in chiral oriented solvents. Anal Chem. 2008;**80**:2963-2972.
[**63**] Canlet C, Merlet D, Lesot P, Meddour A, Loewenstein A, Courtieu J. Deuterium NMR stereochemical analysis of threo–erythro isomers bearing remote stereogenic centres in racemic and non-racemic liquid crystalline solvents. Tetrahedron: Asym, 2000;**11**:1911-1918.
[**64**] Berger R, Courtieu J, Gil RR, C. Griesinger C, Köck M, Lesot P, Luy B, Merlet D, Navarro-Vazquez A, Reggelin M, Reinscheid U M, Thiele C-M, Zweckstetter M. Is the determination of absolute configuration possible by using residual dipolar couplings from chiral non-racemic alignment media?- a critical assessment. Angew Chem Int Ed. 2012;**51**:2-5.
[**65**] Lesot P, Lafon O, Courtieu J, Berdagué P. Analysis of the $^{13}C$ NMR spectra of molecules, chiral by isotopic substitution, dissolved in a chiral oriented evironment: Toward the absolute assignment of the pro-*R*/pro-*S* character enantiotopic ligands in prochiral molecules. Chem Eur J. 2004;**10**:3741-3746,
[**66**] Ziani L, Lesot P, Meddour A, Courtieu J. Empirical Determination of the absolute configuration of small chiral molecules using natural abundance $^{2}H$ NMR in chiral liquid crystals. Chem Commun, 2007;4737-4739.
[**67**] Baillif V, Billault I, Robins RJ, Lesot P. Assignment of absolute configuration of natural abundance deuterium signals associated with (*R*)- and (*S*)-enantioisotopomers in a fatty acid aligned in a chiral liquid crystal: enantioselective synthesis and NMR analysis. J Am Chem Soc. 2006;**128**:11180-11187.

POST-PRINT

[**68**] Serhan Z, Billault I, Lesot P. Recent advances in the analysis of the site-specific isotopic fractionation of metabolites such as fatty acids using anisotropic natural abundance $^{2}H$ NMR spectroscopy: application on conjugated linolenic methyl esters. Anal Bioanal Chem. 2011;**399**:1187-1200.

[**69**] Serhan Z, Martel L, Billault I, Lesot P. Complete determination of site specific bio-enantiomeric excesses in linoleic acid using natural abundance deuterium 2D-NMR in polypeptide mesophase. Chem Commun. 2010;**46**:6599-6601.

[**70**] Baillif V, Robins RJ, Le Feunten S, Lesot P, Billault I. Investigation of fatty acid elongation and desaturation steps in fusarium lateritium by quantitative two-dimensional deuterium NMR spectroscopy in chiral oriented media. J Biol Chem. 2009;**284**:10783-10792.

[**71**] Cahn RS, Inglod CK, Prelog V. The specification of asymmetric configuration in organic chemistry. Experientia. 1956;**12**:81-94.

[**72**] Reed DW, Savile CK, Qiu X, Buist PH, Covello PS, Mechanism of 1,4-dehydrogenation catalyzed by a fatty acid (1,4)-desaturase of Calendula officinalis. Eur J Biochem. 2002;**269**:5024-5029.

[**73**] Serhan Z, Billault I, Borgogno A, Ferrarini A, Lesot P. Analysis of NAD 2D-NMR spectra of saturated fatty acids in polypeptide aligning media by experimental and modeling approaches. Chem Eur J. 2012;**18**:117-126.

[**74**] Zweckstetter M, Bax A, Prediction of sterically induced alignment in a dilute liquid crystalline phase: Aid to protein structure determination by NMR J Am Chem Soc. 2000;**122**:3791-3792.

[**75**] Fernandes MX, Bernado P, Pons M, Garcia de la Torre J. An analytical solution to the problem of the orientation of rigid particles by planar obstacles. Application to membrane systems and to the calculation of dipolar couplings in protein NMR spectroscopy. J Am Chem Soc. 2001;**123**:12037-12047.

[**76**] Abe A, Yamazaki T, Orientational order of alpha-helical poly(gamma-benzyl-glutamate) in the lyotropic liquid-crystalline state - comparison of theory with experiments. Macromol.1989;**22**:2138-2145.

[**77**] Flory PJ, in Statistical Mechanics of Chain Molecules, Wiley Interscience, New York, 1969.

[**78**] Ferrarini A, Modeling of macromolecular alignment in nematic virus suspensions. Application to the prediction of NMR residual dipolar couplings. J Phys Chem B. 2003;**107**:7923-7931.

[**79**] N. Metropolis N, Rosenbluth A,Rosenbluth M, Marshall N, Teller A, Teller E. Equation of state calculations by fast computing machines. J Chem Phys. 1953;**21**:1087-1092.

[**80**] Louhivuori M, Pääkkönen K, Fredriksson K, Permi P, Lounila J, Annila A, On the origin of residual dipolar couplings from denatured proteins. J Am Chem Soc. 2003;**125**:15647-15650.

[**81**] Obolensky OI, Schlepckow K, Schwalbe H, Solov'yov AA, Theoretical framework for NMR residual dipolar couplings in unfolded proteins. J Biomol NMR. 2007;**39**:1-16.

[**82**] Lesot P, Serhan Z, Aroulanda C, Billault I. Analytical contribution of NAD 2D-NMR spectroscopy in polypeptide mesophases to the investigation of triglycerides. Magn Reson Chem. 2012;**50**:S2-S11, and corrigendum, idem, 2013;**51**:444.

[**83**] Robins R, Billault I, Duan J-R, Guiet S, Pionnier S, Zhang B-L. Measurement of $^{2}H$ distribution in natural products by quantitative $^{2}H$ NMR: An approach to understanding metabolism and enzyme mechanism? Phytochem Rev. 2003;**2**:87-102.

[**84**] Schmidt H-L, Werner R, Eisenreich W. Bio-organic chemistry of plant lipid desaturation. Phytochem Rev. 2003;**2**:61-85.

[**85**] Billault I, Ledru A, Ouetrani M, Serhan Z, Lesot P, Robins RJ. Probing substrate-product relationships by natural abundance deuterium 2D-NMR spectroscopy in liquid-crystalline solvents: the case of the epoxidation of linoleate to vernoleate by two different plant enzymes. Anal Bioanal Chem. 2012;**402**:2985-2998.

[**86**] Blée E, Stahl U, Schuber F, Stymne S, Regio- and stereo-electivity of cytochrome P-450 and peroxygenase dependent formation of *cis*-12,13-epoxy-9(*Z*)-octadecenoic acid (vernolic acid) in Euphorbia lagascae. Biochem Biophys Res Commun. 1993;**197**:778–784.

POST-PRINT

[**87**] Lee M, Lenman M, Banas A, Bafor M, Singh S, Schweizer M, Nilsson R, Liljenberg C, Dahlqvist A, Gummeson PO, Sjodahl S, Green A, Stymme S, Identification of non-heme diiron proteins that catalyze triple bond and epoxy group formation. Science. 1998; **280**: 915-918.

[**88**] Berdagué P, Lesot P, Jacob J. Terwilliger VJ, Le Milbeau C. Contribution of NAD 2D-NMR in liquid crystals to the determination of hydrogen isotope profile of methyl groups in Miliacin. Geochim. Cosmochim. Acta. 2016;**173**:337-351.

[**89**] Lafon O, Bingwen H, Amoureux J-P, Lesot P. Fast and high-resolution stereochemical analysis by non-uniform sampling and covariance processing of anisotropic natural abundance 2D $^{2}$H NMR datasets. Chem Eur J. 2011;**17**:6716-6724.

[**90**] Kazimierczuk K, Lafon O., P. Lesot P. Criteria for sensitivity enhancement by compressed sensing: practical application to anisotropic NAD 2D-NMR spectroscopy. Analyst 2014;**139**:2702-2713.

[**91**] Bostock, M, Nietlispach D. Compressed sensing: Reconstruction of non-uniformly sampled multidimensional NMR data. Concepts Magn Reson, A, 2017;**46A**:1-19, Special Issue, Article Number: e21438.

[**92**] Kazimierczuk K. Compressed sampling in NMR spectroscopy. eMagRes. 2018; **7**:1-8.

POST-PRINT